



Canadian Geotechnical Journal

Using DEM to create a CPT based method to estimate the installation requirements of rotary installed piles in sand

Journal:	<i>Canadian Geotechnical Journal</i>
Manuscript ID	cgj-2020-0017.R1
Manuscript Type:	Article
Date Submitted by the Author:	n/a
Complete List of Authors:	Sharif, Yaseen; University of Dundee, Geotechnical Brown, Michael; University of Dundee Ciantia, Matteo Oryem; University of Dundee, Cerfontaine, Benjamin; University of Dundee Davidson, Craig; University of Dundee, School of Science and Engineering Knappett, Jonathan; University of Dundee, Civil Engineering Meijer, Gerrit; University of Dundee; University of Bath Ball, Jonathan; Roger Bullivant Ltd
Keyword:	DEM, Rotary installation, Silent piling, Installation requirements, CPT
Is the invited manuscript for consideration in a Special Issue? :	Not applicable (regular submission)

SCHOLARONE™
Manuscripts

Date of resubmission: 05/08/2020

Date of first submission: 03/06/2020

Title: Using DEM to create a CPT based method to estimate the installation requirements of rotary installed piles in sand

Author list

Yaseen Umar Sharif*, Michael John Brown, Matteo Oryem Ciantia, Benjamin Cerfontaine, Craig Davidson, Jonathan Knappett, Gerrit Johannes Meijer, Jonathan Ball

**Corresponding author*

Author details

Yaseen Umar Sharif, MEng

PhD student, School of Science and Engineering, University of Dundee, Fulton Building, Dundee, DD1 4HN, UK

ORCID: 0000-0002-3620-7500

Email: y.u.sharif@dundee.ac.uk

Michael Brown, BEng PhD GMICE

Reader, School of Science and Engineering, University of Dundee, Fulton Building, Dundee, DD1 4HN, UK

ORCID: 0000-0001-6770-4836

Email: m.j.z.brown@dundee.ac.uk

Matteo Oryem Ciantia,

Lecturer, School of Science and Engineering, University of Dundee, Fulton Building, Dundee, DD1 4HN, UK

ORCID: 0000-0003-1897-4471

Email: m.o.ciantia@dundee.ac.uk

Benjamin Cerfontaine, BSc, MSc, PhD

MSCA Research Fellow, School of Science and Engineering, University of Dundee, Fulton Building, Dundee, DD1 4HN, UK

ORCID: 0000-0002-4833-9412

Email: b.cerfontaine@dundee.ac.uk

Craig Davidson, BSc MSc

Research Associate, School of Science and Engineering, University of Dundee, Fulton Building, Dundee, DD1 4HN, UK

ORCID: 0000-0002-4843-5498

Email: c.s.davidson@dundee.ac.uk

Jonathan Adam Knappett, MEng (Hons), PhD

Professor, School of Science and Engineering, University of Dundee, Fulton Building, Dundee, DD1 4HN, UK

ORCID: 0000-0003-1936-881X

Email: j.a.knappett@dundee.ac.uk

Gerrit Johannes Meijer, BSc, MSc, PhD

Postdoctoral Research Associate, School of Science and Engineering, University of Dundee, Fulton Building, Dundee, DD1 4HN, UK

ORCID: 0000-0002-2815-5480

Email: g.j.z.meijer@dundee.ac.uk

Jonathan David Ball, BSc, CGeol, FGS

Chief Geotechnical Engineer, Roger Bullivant Ltd, Burton Upon Trent, UK

Main text word count: 9295

Number of tables: 4

1 **Number of Figures:**13

2

Draft

3 **Using DEM to create a CPT based method to estimate the installation requirements of rotary**
4 **installed piles in sand**

5 Yaseen Umar Sharif*, Michael John Brown, Matteo Oryem Ciantia, Benjamin Cerfontaine, Craig
6 Davidson, Jonathan Knappett, Gerrit Johannes Meijer, Jonathan Ball

7

8 **Abstract**

9 Deep foundations maybe used in a range of soil types where significant foundation resistance is
10 required but their installation is often associated with disturbance due to noise and vibration. Greater
11 restrictions on use in urban and offshore environments is now commonplace. Screw piles and rotary
12 jacked straight shafted piles are two potential methods of silent piling that could be used as alternative
13 foundation solution, but the effects of certain geometric and installation properties such as
14 installation pitch i.e. the ratio between vertical displacement and rotation, on the required installation
15 torque and force in sand are not well understood. In this paper the effects of installation pitch and
16 base geometry on the installation requirements of a straight shafted pile are simulated in 3D using the
17 discrete element method (DEM). The installation requirements of straight shafted piles into sand have
18 been validated against centrifuge testing, in three different relative densities. The DEM shows
19 reductions in installation force can be achieved by increasing the installation pitch or including a
20 conical tip. An existing cone penetration test (CPT) based prediction method for installation
21 requirements has been improved to include the effects of installation pitch and base geometry for
22 rotary installed piles in sand.

23 **Keywords**

24 DEM, Rotary installation, Silent piling, Installation requirements, CPT

25

26 1 Introduction

27 Deep foundations may be used in a range of soil types where significant foundation resistance is
28 required but, depending on the pile type, their installation may be associated with environmental
29 disturbance due to noise and vibration e.g. in classic pile driving. In the urban environment, noise
30 pollution is usually restricted to specific times of day and vibrational sources are limited in minimum
31 separation from specialist equipment in building such as hospitals and laboratories (BS5228, 1992). As
32 well as limitations onshore, legislation and restrictions on the allowable level of noise generated when
33 installing deep foundations have recently been introduced by countries involved in offshore
34 renewable energy development (Huisman, 2019). These restrictions are designed to limit the
35 disturbance to marine mammals, but there is a trend to increase foundation size and capacity
36 (Golightly, 2014) which may make it more challenging to meet existing and future environmental
37 controls. Therefore, current onshore “silent” piling methods are being investigated to aid in the
38 development of potential offshore “silent” piling techniques.

39 Several methods have been developed to mitigate the noise problem especially in urban
40 environments through alternative pile construction techniques such as continuous flight auger (CFA)
41 (Mandolini *et al.*, 2002), bored displacement piles such as the continuous helical displacement pile
42 (CHD) (Jeffrey *et al.*, 2016), the press-in piling method (White and Deeks, 2007) and rotary press-in
43 method (Deeks and White, 2008) and screw piles (Lutenegger, 2009). If current onshore “silent” piling
44 techniques are exported to the offshore environment many factors need to be considered. The CFA
45 and CHD piling method do not lend themselves to offshore installation as both methods require the
46 pile to be cast in-situ using concrete. This limits the available “silent” construction methods to steel
47 displacement piles, such as a tubular piles installed using the press-in or rotary press-in methods or
48 screw piles. In offshore applications the foundation options would be required to resist larger forces,
49 both axially and horizontally. Davidson *et al.*(2020) have suggested that for large jacket structures
50 installed in a water depths up to 80m, an individual pile installed at one corner of a jacket structure

51 may be required to resist axial compressive and tensile forces of up to 35MN and 26MN respectively,
52 with an associated horizontal load of 6MN. This will result in a need to significantly increase the
53 current sizes of the piles, in terms of both capacity requirements but also structural section sizes. This
54 increase in size raises concerns over the ability to install the steel displacement piles using the
55 aforementioned methods where Davidson *et al* (2020) suggested vertical installation or crowd forces
56 of up to 22MN in 84% density sand where pitch matched installation of screw piles was used. This
57 raises concerns over the large vertical compressive forces that would be required during installation
58 and practical challenges of creating large capacity load reaction systems in the offshore environment.
59 Thus, where possible it would be advantageous to reduce vertical or crowd installation forces where
60 there is greater ability to control or vary the torque input as required. For example, previous work by
61 Deeks and White (2008) has shown that by using the rotary press-in method and varying the approach
62 to installation, the installation force required to install a tubular pile can be significantly reduced. Both
63 rotary press-in piles and the screw piles are installed in a similar way, through the application of
64 rotational and vertical displacement with the only difference being the addition of helices to the screw
65 pile.

66 The necessary increase in pile size limits the ability to predict the installation requirements, of both
67 techniques, in terms of torque and vertical force ("crowd force"), which may not be adequately
68 captured by current analytical and empirical based approaches (Davidson et al., 2018). In addition to
69 this, the effects of geometry and installation properties such as installation pitch (P_i) (the ratio
70 between vertical (\dot{w}) and rotational or angular ($\dot{\theta}$) velocity) (Equation 1) on the required installation
71 torque and force have seen little previous attention.

$$P_i = \frac{\dot{\theta} d_c}{2\dot{w}} \quad (1)$$

72 where d_c is the diameter of the pile shaft or core. As the geometry of a screw pile is complex, with the
73 addition of helices, this paper will focus on the effect of P_i on the installation requirements of a straight
74 shafted pile.

75 Currently there are no existing methods focusing on predicting the installation requirements of rotary
76 installed straight shafted piles. Several methods for the predicting installation requirements have been
77 developed for screw piles, with the majority focusing on the prediction of installation torque. Some of
78 these methods split the geometry of the pile into component parts (helix, base and shaft), which
79 allows them to be modified to create a prediction method for the installation requirements of rotary
80 installed straight shafted piles.

81 For instance Ghaly and Hanna (1991) and Sakr, (2015) developed analytical methods for predicting
82 torque which split the installation torque into components based upon geometric features of the
83 screw pile (helices and shaft). These approaches have a tendency to overpredict installation
84 requirements (Davidson *et al.*, 2020) and may have limited validation. For example, the Ghaly and
85 Hanna (1991) method, for predicting installation force and torque, was developed through 1g model
86 testing in dry sand and has limited field test verification. The Sakr (2015) procedure has been validated
87 against some limited field scale tests, but with relatively small geometries in comparison to those
88 proposed by Davidson *et al.*(2020).

89 Prediction methods based upon in-situ cone penetration tests (*CPT*) have been shown to be potentially
90 more reliable, due to the availability of continuous data logging along the path of installation and the
91 full displacement nature of the *CPT* test. Existing *CPT* design methods are typically used to predict the
92 installation torque of screw piles (Gavin *et al.*, 2013; Spagnoli, 2017; Davidson *et al.*, 2018), with a
93 single method proposed for associated installation force by Al-Baghdadi (2017). A common
94 assumption in all of these methods is that the screw piles are installed at P_i that matches the geometric
95 pitch (P_g) of the helix, so that for each rotation the screw pile displaces one P_g vertically. This is referred
96 to as pitch matched or “perfect” installation by Lutenegger (2019). The methods do not consider the
97 effects of P_i on the base and shaft components.

98 Previous studies on rotary installed straight shafted piles in very dense sands (Deeks and White, 2008;
99 Ishihara *et al.*, 2015) have shown that by altering the installation pitch, the vertical force required to

100 install a straight shafted pile can be reduced, but knowledge regarding the effects at other relative
101 densities is limited. Al-Baghdadi (2017) investigated the installation requirements of a straight shafted
102 pile with a conical tip in different relative densities at a single installation pitch. The results showed
103 that the percentage reductions in vertical compressive force with the application of rotation, were
104 density dependent.

105 Through the use of discrete element modelling (*DEM*) calibrated against triaxial and centrifuge tests,
106 the effect of installation pitch on the installation requirements of straight shafted piles is assessed in
107 this paper and guidance is given on how to optimise the pile geometry and installation pitch in order
108 to reduce the installation requirements. The simulations took place in soils at three different relative
109 densities in sand. Using the results of the simulations, an improvement to the existing *CPT* based
110 design method for predicting installation torque and force proposed by Davidson *et al.* (2018) and Al-
111 Baghdadi (2017) respectively are made to include the effects of varying installation pitch and pile base
112 geometry.

113 **2 Methodology used in discrete element method simulation**

114 The discrete element method (*DEM*) is a numerical modelling framework which can be used to
115 simulate large deformation problems in granular soils (Arroyo *et al.*, 2011). Rather than using a
116 continuum to model the soil as finite element analysis (*FEA*) does, the *DEM* uses discrete particles that
117 are able to interact to represent the soil body. *DEM* has been previously used to model a variety of
118 different soil-structure interaction problems including pile plugging (Liu *et al.*, 2019), cone penetration
119 tests (Butlanska *et al.*, 2014) and jacked piles in sand (Ciantia *et al.*, 2019). With the application of an
120 increase gravitational field, the *DEM* is able to act as a virtual centrifuge (Ciantia *et al.*, 2018) which
121 when properly calibrated, has the added benefit of using a single soil chamber which can be reset and
122 used multiple times. This allows for direct comparisons to be made in parametric studies and

123 potentially removes the reliance on specialist laboratory facilities or comparisons to expensive field
124 studies, where soil variability can be an issue with interpretation.

125 To model the installation of the straight shafted piles, Particle Flow Code 3D 5.0.35 (Itasca Consulting
126 Group, 2016) was used alongside a simplified Hertz-Mindlin contact model (Mindlin and Deresiewicz,
127 1953). The parameters for the soil–soil and soil-structure interaction, were calibrated against
128 laboratory triaxial and centrifuge tests respectively (Sharif *et al.* 2019a) and validated against
129 centrifuge tests of straight shafted piles (Sharif *et al.* 2019b) and screw pile (Sharif *et al.* 2019a)
130 geometries. Further details on the calibration and validation of the contact models used within this
131 study can be found in Sharif *et al.* (2019a) and are outlined in Table 1. The sand modelled in the
132 simulations is based upon the properties of HST95, which is a medium to fine well graded sand that is
133 commonly used at the University of Dundee in physical modelling and element testing with the
134 behaviour and properties of the soil being previously investigated and well documented (e.g. Al-Defae
135 *et al.*, 2013; Lauder *et al.*, 2013). Frictional rigid boundaries (walls) were used to model the straight
136 shafted pile. The model scale pile had a diameter of 10mm, a length of 200mm and a tip with an apex
137 angle of 60 degrees (Figure 1a). Using a gravitational acceleration of 50g, the prototype scale of the
138 pile is 0.5m diameter and an installation depth of 10m. The calculated results from the simulations
139 were scaled in accordance with centrifuge scaling laws (Garnier *et al.*, 2007), such that the length is
140 multiplied by N force by N^2 and torque by N^3 , where N is the model scaling factor ($N=50$). For the DEM
141 implementation of the structure, the pile was split into base and multiple shaft components. The 10
142 mm diameter model scale *CPT* used within this study was segmented such that it mimicked the
143 instrumentation of a cone penetrometer i.e. there is a “sleeve” of length $4 d_c$ behind the cone which
144 is used to calculate the sleeve friction (f_s).

145 The virtual soil chambers for the DEM analysis were created in accordance with the specification in
146 Sharif, *et al.* (2019b), which implements the particle refinement method (*PRM*) (McDowell *et al.*, 2012),
147 which is a similar process to mesh refinement commonly used in *FEA* (Figure 1b). This methodology

148 has previously been implemented by McDowell *et al* (2012) and Shi *et al.*(2019). Three soil chambers
149 were created in this manner each having a different relative density (D_r). The relative densities chosen
150 were 32%, 55% and 73% in line with the centrifuge tests on straight shafted piles conducted by Al-
151 Baghdadi (2017). The dimensions and properties of the soil chambers can be seen in Table 2. To avoid
152 any boundary effects, the radius of the soil chamber was made to be greater than the $20R$ as suggested
153 by Bolton *et al* (1999), where R is the radius of the pile. Figure 2 shows the mean effective stress (σ')
154 profile with depth at different radial distances from an installed pile in the dense soil bed. It can be
155 seen that at a radial distance of $20R$ there is no significant change in mean effective stress compared
156 to the initial soil conditions confirming adequate model sizing.

157 To reduce the run-time of the simulation, a particle size distribution (*PSD*) scaling value (n_i) of 20 was
158 adopted. This value represents the multiplier applied to the diameter of particles, so that each particle
159 now represents n_i^3 particles with the bulk properties of the soil remaining the same. The particle
160 scaling of 20 at the centre of the chamber was selected based upon the minimum recommended ratio
161 of diameter of the pile (d_c) over the median particle size (d_{50}) of 2.69 (Arroyo *et al.*2011). To limit the
162 possibility of particle migration between scaling zones, the increase in the *PSD* scaling value (n_i),
163 between adjacent concentric zones, was limited to 1.35 for this soil type, such that the smallest
164 particle (d_{00}) of the larger scale is smaller than the median particle in the smaller scale. A maximum n_i
165 of 120 was selected at the boundaries. An example soil chamber can be seen in Figure 1b. Where the
166 shading of the particles represents different values of n_i . The variable scaling values, shown in Figure
167 1b, are consistent across all soil beds used within this study The gravitational field of the chamber was
168 set at 50g to match the centrifuge tests of Al-Baghdadi (2017). Table 3 outlines all of the simulations
169 conducted in this study.

170 3 Results

171 3.1 Overview of the reductions in total Installation force and increase in total 172 installation torque with an increase in installation pitch

173 Figure 3 shows the global reduction in total vertical compressive force and the increase in torque with
174 an increase in installation pitch. A 300-point adjacent averaging of the 80,000 point output data with
175 a reflective end constraint, was used to reduce the level of noise in the outputs from *DEM* simulation,
176 which was produced by the particle scaling. Results show that the total vertical force is reduced, and
177 the total torque is increased as the installation pitch increases. By separating out the contribution of
178 the total force and torque produced by the base and the pile shaft on the straight shafted pile, it is
179 shown (Table 4) that the vertical resistance is primarily produced by the base of the pile and the torque
180 by the shaft for all densities and at all installation pitches. During a monotonic push ($P_i = 0$), 75% of
181 the vertical force, generated during installation, is attributed to the base of the pile. Therefore, to
182 reduce the installation force in sand, it is much more important to reduce the base component of
183 force rather than the shaft. These effects will be studied in detail in the following section.

184 3.2 Reduction in installation force due to increase in installation pitch

185 Consideration of the results is undertaken with a view to improving the shaft and base component
186 terms in the existing *CPT* based installation prediction techniques for rotary pile installation (Al-
187 Baghdadi, 2017; Davidson *et al.*, 2018) where these methods are broken down into force and torque
188 predictions based upon *CPT* cone resistance (q_c). To assess whether the percentage reduction in
189 vertical force due to varying P_i is consistent across different relative densities, the base resistance (q_b)
190 and the vertical component of shaft resistance (τ_{sv}) (Figure 4) were normalised by the *CPT* cone
191 resistance (q_c) from a 10mm model scale (0.5m prototype scale) virtual *CPT* conducted in each of the
192 50g *DEM* chambers. The normalised resistance was then plotted against P_i (Figure 5). Figure 5a shows
193 that at high installation pitches ($P_i > 8$) the application of rotation causes a 34% reduction in the base

194 resistance. Whereas for the shaft resistance an average decrease of 85% was achieved (Figure 5b) with
 195 small variations in normalised shaft resistance occurring between densities. Thus, changing the
 196 distribution of total vertical force during rotary installation from 75% to 94% at the base and from 25%
 197 to 6% on the shaft.

198 From Figure 5a the reductions in normalised base resistance are consistent across all three relative
 199 densities for all installation pitches. At high installation pitches it appears that the normalised base
 200 resistance is asymptotic to 0.66 (34% reduction). The asymptote can be used to assess how resistance
 201 is produced at the base of the pile during installation. During a monotonic push ($P_i = 0$) full soil
 202 resistance is mobilised and it is assumed that the soil is flowing around the base of the pile as it
 203 advances. As the pile advances, frictional resistance would form at the interface of the base and the
 204 soil. The vertical component of this shear stress would contribute to q_b . When the pile is rotated ($P_i >$
 205 0), the direction in which the base shear stress (τ_b) acts, rotates accordingly (Figure 4). Thus, the
 206 vertical component (τ_{bv}) would reduce, and the tangential component (τ_{bt}) would increase (Figure 4).
 207 At high installation pitches ($P_i > 8$) τ_b would act primarily in the tangential direction, with very little
 208 frictional/shear resistance acting vertically. This would result in a reduction of q_b , with the percentage
 209 reduction representing the proportion of base resistance due to friction. Thus, it can be stated that
 210 34% of q_b at $P_i = 0$ is produced through interface friction, for the geometry shown in Figure 1a. The
 211 reduction in the base resistance as P_i increases, can be expressed as:

$$\frac{q_b}{q_c} = \frac{1}{\sqrt{1 + (P_i + 2.5)^2}} + b \quad (2)$$

212 where q_b is the base resistance of the pile, q_c is the cone resistance from a *CPT* and b is the percentage
 213 base resistance other than from friction (0.66). Equation 2 appears to capture the reduction in base
 214 resistance well (Figure 5a) for all installation pitches and densities.

215 The normalised base resistance results suggest that rotary installing straight shafted piles, at $P_i < 4$ is
 216 not ideal. Low installation pitches in practice are difficult to maintain and appear to yield low

217 reductions in base resistance. It is much more optimal to install at $P_i > 8$ as this reduces the base
 218 resistance by approximately 34% from the $P_i = 0$ case.

219 The normalised shaft resistance (Figure 5b) shows some small variations between the relative
 220 densities, with the difference being more apparent at low installation pitches ($P_i < 4$). As discussed by
 221 White and Deeks (2007), the radial stress regime (σ_r) on the pile shaft is caused by unloading of the
 222 soil in contact with the shaft, after it has passed around the base of the advancing pile. Jardine *et al*
 223 (1993) have shown that the radial stress (σ_r) regime on the shaft of the pile is both density and depth
 224 dependent. Therefore, leading to small variations when normalising by q_c . Continuing with the analogy
 225 of a displacement pile, at $P_i = 0$, being similar to *CPT*, the shaft resistance (τ_s) of the pile is comparable
 226 to the sleeve friction (f_s) of a *CPT*. τ_s on a displacement pile is commonly defined by equation 3:

$$\tau_s = \sigma_r \tan \delta \quad (3)$$

227 where τ_s is the shaft resistance, σ_r is the radial stress on the shaft during installation and δ is the
 228 interface friction angle. Rearranging Equation 3 gives:

$$\sigma_r = \frac{\tau_s}{\tan \delta} \quad (4)$$

229 From the *DEM* simulations it can be determined that σ_r on the pile is the same as σ_r on a *CPT* (Figure
 230 4c) as suggested by White and Deeks (2007) and Lehane *et al.* (2005). It is therefore possible to relate
 231 τ_s to f_s through σ_r . f_s can be related to q_c through the *CPT* friction ratio ($F_r = f_s/q_c$):

$$\tau_s = f_s \frac{\tan(\delta_{pile})}{\tan(\delta_{CPT})} = a q_c \tan \delta_{pile} \quad (5)$$

$$a = \frac{F_r}{\tan \delta_{CPT}} \quad (6)$$

232 where a is the stress drop index (Lehane *et al.*, 2005; Schneider *et al.*, 2007), δ_{CPT} and δ_{pile} are the
 233 interface friction angles of the *CPT* and the pile respectively. Direct comparison between f_s and τ_s is
 234 not recommended (White and Deeks, 2007), due to the lack of confidence in sleeve friction
 235 measurements which may be affected by misalignment and wear over time. From the *CPT*

236 classification charts proposed by Robertson *et al.* (1986) it is shown that F_r of a *CPT* changes with soil
 237 type, but also that small changes in F_r occur in sands of different relative densities, resulting in
 238 different values of α . The values of F_r for the *CPTs* from this study range between 0.75% and 1.05%,
 239 which results in a 25% difference in the value of the stress drop index. If the shaft resistance is then
 240 normalised using $\tau_{sv}/(aq_c \tan \delta_{pile})$ (Figure 5c) the small density effect seen in Figure 5b is removed.
 241 The additional data shown in Figure 5c will be discussed at a later stage in this paper.

242 With the application of rotation ($P_i > 0$), the direction of τ_s is no longer purely vertical. Therefore, the
 243 shear stress has both a vertical component (τ_{sv}) and a tangential component (τ_{st}) (Figure 4). τ_{sv}
 244 contributes to the vertical force and τ_{st} contributes to installation torque. Assuming σ_r is constant for
 245 all values of P_i , in a given density, the relationship between τ_{sv} and P_i can be expressed using simple
 246 trigonometry leading to equation 7 (Figure 5c).

$$\frac{\tau_{sv}}{aq_c \tan \delta_{pile}} = \frac{1}{\sqrt{1 + P_i^2}} \quad (7)$$

247 As the measurements of *CPT* sleeve friction and therefore F_r are not always considered reliable, as
 248 previously discussed, the value of the stress drop index can be assumed to be fixed. In the UWA-05
 249 design method for driven piles in sand (Lehane *et al.*, 2005) it is recommended that $\alpha=0.03$ ($F_r=1\%$) for
 250 piles loaded in compression. The fixed value maybe deemed as an acceptable approach as the shaft
 251 component of vertical force is small in sand for all installation pitches.

252 3.3 Increase in installation torque with an increase in installation pitch

253 As well as considering the vertical force requirements for installation, the existing *CPT* prediction
 254 methods also consider torque separately (Davidson *et al.*, 2018). Installation torque is generated
 255 during rotary installations by a tangential force acting at a lever arm from the centre of the pile (Figure
 256 4). The tangential force is generated by the tangential component of the shear stress at the interface
 257 between the pile and soil. To normalise the base component of the installation torque (T_b), T_b is divided
 258 by $q_c A_b \bar{R}$ where A_b is the surface area of the base and \bar{R} is the equivalent radius of the pile base. The

259 shaft component of installation torque (T_s) can be expressed as the tangential component of shear
 260 stress acting over the surface area of the shaft (A_s) with a lever arm of the radius of the pile (R). To
 261 then normalise the shaft component of torque, T_s is divided by $\tau_s A_s R$, where τ_s is defined by equation
 262 5, A_s is the surface area of the shaft. The normalised base and shaft torque can be seen in Figure 6.

263 The proportion of the total installation torque that is produced by the base of the pile is relatively low.
 264 This is due to the small surface area associated with base geometry and the variable lever arm that
 265 increases linearly from 0 to R moving up the pile tip. From the normalised base torque (Figure 6a), all
 266 three densities show the same trend. At $P_i > 4$ the value of the normalised torque reaches a limit of
 267 0.34. This agrees with results from the reduction in vertical resistance. Both the normalised base
 268 torque and force suggest that 34% of base resistance, for the geometry shown in Figure 1a, during a
 269 monotonic push in sand is produced through interface friction. The increase in normalised torque can
 270 be expressed as per equation 8 (Figure 6a):

$$\frac{T_b}{q_c A_b \bar{R}} = \frac{(1-b)P_i}{\sqrt{1+P_i^2}} \quad (8)$$

271 When the normalised shaft torque is plotted against the installation pitch (Figure 6b), a distinct density
 272 effect can be seen. The asymptotic value of normalised torque for each density varies. Installation
 273 torque is produced through interface friction, which for the shaft is governed by the radial stress that
 274 acts on the shaft of the pile. The normalisation method used in Figure 6b applies a variable stress drop
 275 index (α) and therefore represents the radial stress that acts on the pile at $P_i = 0$. As the asymptotic
 276 value is not 1 for any of the densities, a reduction in radial stress on the shaft of the pile has occurred
 277 when it is rotated, and the percentage reduction is density dependent.

278 3.4 Effect of installation pitch on the radial stress and particle displacement

279 To assess the change in radial stress along the shaft of the pile, the particle-wall contact forces for
 280 each individual section of the segmented pile are assessed at the end of the installation process (Figure
 281 7). The percentage reduction in radial stress on the shaft of the pile installed into the loose soil

282 chamber is much higher than the percentage reduction of the radial stress in the dense soil. This
283 confirms that the radial stress on the shaft of a pile reduces, if the pile has been rotated, and the
284 percentage reduction of radial stress is density dependant.

285 The reduction in radial stress is thought to be caused by the rotation of the principle stress, which in
286 turn change the direction of shearing within the soil. This would result in the principal strain direction
287 of the soil to changing accordingly. This has previously been shown in torsional shear tests of hollow
288 cylinder samples of granular material (Tatsuoka *et al.*, 1986), where it was shown that the principle
289 strain direction under torsional shearing is inclined between the tangential and vertical direction. In
290 the $P_i = 0$ case the direction of shearing, along the shaft of the pile, is primarily in the vertical direction.
291 Therefore, the principle strain direction is perpendicular to the shaft of the pile, or in other words the
292 soil attempts to move in the radial direction. The soil movement is restricted by the rigid shaft of the
293 pile, resulting in large radial stresses.

294 When the pile is rotated during installation ($P_i > 0$), the direction of the principle stresses within the
295 soil are assumed to also rotate accordingly. The rotation of the principle stresses results in the
296 direction of shearing no longer being purely in the vertical direction. The direction of shearing when
297 $P_i > 0$ is assumed to be inclined between the vertical and tangential directions. As a result, the principle
298 strain direction would be perpendicular and therefore no longer be purely in the radial direction. The
299 pile would therefore only experience a projection in the radial direction of the stresses induced by the
300 particle displacement. Which ultimately appears as a reduction in the radial stress on the shaft of the
301 pile.

302 The difference in percentage reduction of the radial stress seen in the different relative densities
303 (Figure 7), is most likely due to the volume of void space and particle packing that is present for a given
304 density, and how this facilitates the movement of particles during shearing. To assess the effect of
305 installation pitch on particle displacement around the pile during installation, the Cartesian
306 coordinates of the individual particles were extracted before and after an imposed vertical

307 displacement of 0.25 m. The initial location of each particle of interest was then plotted onto a scatter
 308 graph and shaded in accordance with its magnitude of displacement in the polar axis being
 309 investigated (Figure 8). In loose soil it is much easier for the individual soil particles to displace into a
 310 void and for a volume of loose soil to contract under shearing. With the direction of the shear band
 311 being inclined, when $P_i > 0$, the soil movement would no longer be restricted by the rigid pile shaft
 312 (Figure 8a & b). Which should allow for much more particle displacement to occur in the tangential
 313 direction (Figure 8b) and result in a larger reduction in radial stress. In dense soils there is much less
 314 void space for particles to displace in to. Therefore, during the shearing process the direction of the
 315 shear band has little effect on the principle strain direction (and therefore particle displacement) and
 316 the soil dilates to accommodate the volume of the pile (Figure 8c and 8d). As a result, the reduction
 317 in radial stress is highly density dependent, with larger reductions occurring in loose soil and smaller
 318 reductions in denser soils. This reduction in radial stress during the installation process of rotary
 319 installed piles has previously been reported in the centrifuge tests of both Deeks (2008) and Al-
 320 Baghdadi (2017). Al-Baghdadi (2017) also suggested that the reduction in radial stress was density
 321 dependent with, with denser soils having a lower percentage decrease in radial stress than looser soils,
 322 as also shown by the DEM results.

323 Using the difference in normalised torque from Figure 6b and Figures 7a-7c for the three different soil
 324 chambers, it is possible to plot the rotation reduction factor (f) against relative density (Figure 7d).
 325 The relationship shown in Figure 7d appears linear and can be expressed as:

$$f = 0.73D_r + 0.3 \quad (9)$$

326 Including f in the normalisation of the shaft component of installation torque (Figure 9), removes the
 327 density effect seen in Figure 6b. The relationship between T_s and P_i can be expressed by equation 10:

$$\frac{T_s}{afq_c A_s R} = \frac{P_i}{\sqrt{1 + P_i^2}} \quad (10)$$

328 The normalised installation torque has shown that at $P_i > 4$ the installation torque does not appear to
329 increase. Whereas for the installation force, the reductions in normalised base resistance becomes
330 asymptotic at $P_i > 8$. Which in practice means it is much more beneficial to install piles at $P_i > 8$ as there
331 is still potential to reduce the installation force without increasing installation torque.

332 3.5 Comparison of DEM results to previous studies on rotary installed piles

333 To assess whether the results of the *DEM* simulations give the same relationships as observed in
334 independent physical model tests, the results were compared to the centrifuge tests conducted by
335 Deeks (2008) in very dense sand ($D_r = 84\%$). The pile used in the centrifuge tests was an instrumented
336 close ended flat based pile. To make the results of the DEM simulations comparable to those of Deeks
337 (2008), the normalisation of the base component of installation force and torque no longer uses the
338 cone resistance q_c , as this information is not available for the tests conducted by Deeks (2008). In place
339 of q_c the base resistance of the pile during monotonic push ($P_i = 0$) is used and notated as $q_{b,0}$. For the
340 shaft, the normalisation can remain the same as τ_s is used by Deeks (2008) which can be expressed as
341 $\alpha q_c \tan \delta$. Using equation 9, the radial stress reduction factor can also be obtained for the centrifuge
342 tests, as D_r is known.

343 The normalised DEM results for the shaft component of installation force and torque are in agreement
344 with the physical model tests (Figure 5c & 9). The relationships between the normalised installation
345 requirements and P_i expressed in equations 7 & 10 fit the trend of the centrifuge tests well. However,
346 when comparing the normalised base components of installation force and torque, a large difference
347 can be seen between the DEM and centrifuge results presented by Deeks (2008) (Figure 10). The DEM
348 simulations show much larger reductions in normalised base resistance during rotary installation, and
349 lower increases in normalised torque. It is assumed that the difference in geometry between the pile
350 used in the centrifuge tests (flat base) and the one used in the DEM simulations (60° cone) causes the
351 difference in normalised installation requirements.

352 4 Development of an Analytical model to predict the base component 353 of installation force and torque

354 With the assumption of normal stress (σ_n) acting along the interface of the pile base, two components
355 contribute to vertical resistance (Figure 4 & 11a). The first contributor is the vertical component of the
356 normal stress. The second is frictional in nature and is the vertical component of the base shear stress
357 (τ_b) induced by σ_n . Assuming that σ_n does not change when the pile is rotated and that τ_b rotates in
358 accordance with the Installation pitch, an analytical solution can be obtained for the installation
359 requirements of the base of the pile. The full derivation of the analytical solution can be seen in the
360 supplementary data for this paper. The variation of force and torque compared to $q_{b,0}$ predicted by
361 the analytical solution can be expressed as:

$$\frac{q_b}{q_{b,0}} = \frac{\tan\beta}{\tan\beta + \tan\delta} + \frac{2\tan\delta \cos\beta}{(\tan\beta + \tan\delta)\sqrt{\cos^2\beta + P_i^2 + \cos\beta}} \quad (11)$$

$$\frac{T_b}{q_{b,0}A_b\bar{R}} = \frac{2\tan\beta \tan\delta}{\tan\beta + \tan\delta} \left[\left[1 - 2\left(\frac{\cos\beta}{P_i}\right)^2 \right] \sqrt{1 + \left(\frac{\cos\beta}{P_i}\right)^2} + 2\left(\frac{\cos\beta}{P_i}\right)^3 \right] \quad (12)$$

362 where β is half of the apex angle of the pile base (Figure 11a). For a flat base $\beta = 90^\circ$ and $\beta = 0^\circ$ would
363 represent an infinitely tall cone.

364 To test the applicability of the analytical model (Equations 11 and 12), a series of DEM simulations
365 were conducted using a straight shafted pile with different base geometries in the dense soil chamber.
366 The apex angle of the base of the pile were varied from 20° to 80° as well as a flat base case (Table 3).
367 To be able to evaluate the reduction in base resistance when the pile is rotated, each of the piles were
368 installed at $P_i = 0$ and 4. To compare the base resistance of each pile, a shape function (S) is required.
369 S can be formulated by comparing $q_{b,0}$ to q_c and can be seen in (Figure 11b). The relationship between
370 the normalised base resistance and the apex angle appears to be linear and can be expressed as:

$$S = \frac{q_{b,0}}{q_c} = 0.014\beta + 0.55 \quad (13)$$

371 The results in Figure 11b show that larger apex angles produce much more resistance to penetration,
 372 with a flat base having the largest. This is expected as, during full flow conditions, a flat base is
 373 assumed to form a cone of sand in front of itself in order to displace the soil radially (White *et al.*,
 374 2005). The sand cone would result in soil- soil shear along the interface, which would increase the
 375 resistance to installation. A similar phenomenon was also shown in the work of Coyne and Lewis
 376 (1999), when investigating seabed ploughs. Their tests showed that nearly double the force was
 377 required when laterally displacing a flat wall in comparison to a plough blade with an angle of 40°. This
 378 in itself would suggest that to reduce installation force for a rotary installed pile, such as a screw pile,
 379 a conical base would be much more beneficial than a flat base.

380 To deduce the percentage reduction in base resistance for the different geometries when the pile is
 381 rotated, q_b of the piles installed at $P_i = 4$ can be normalised by Sq_c and plotted against the β (Figure
 382 11c). Figure 11c shows that smaller apex angles, have larger scope for reduction in vertical resistance.
 383 The analytical model for the reduction in vertical resistance (Equation 11) shows a good comparison
 384 to DEM results (Figure 11c), although the DEM results show a small variation against the analytical
 385 model for the flat base. The analytical solution expressed in equation 11 assumes that there is no loss
 386 in normal stress when the pile is rotated and reductions in vertical base resistance only occur on the
 387 vertical component of shear stress. For a flat base the normal stress is perpendicular to the surface of
 388 the base and therefore there is no vertical component of shear stress. If there is no vertical component
 389 to τ_b , then the analytical model will result in no reductions in base resistance. As a result, Equation 11
 390 is unable to predict the reduction in vertical base resistance for a flat base, which is seen in both the
 391 DEM and centrifuge tests of Deeks (2008). The most likely explanation for the reduction in base
 392 resistance for the flat base is a change in geometry of the soil cone (as shown in Figure 12) when the
 393 pile is rotated compared to a monotonic push, as proposed by Deeks (2008). Figure 12 shows the
 394 magnitude of average particle displacement (U) for a flat based pile, installed at $P_i = 0$ and 4. For the

395 $P_i = 0$ case the shape of the nose cone is conical in nature and extends vertically by $2 d_c$ and radially by
396 $1.5 d_c$. In contrast to this the nose cone of the pile installed at $P_i = 4$, the vertical and radial extent of
397 the nose cone are $1.6 d_c$ and $2.0 d_c$ respectively. It is therefore recommended that the analytical
398 solution is not used to predict the reduction in base resistance for a flat base and a 10% reduction in
399 base resistance for piles installed at $P_i > 4$ is used for flat based piles. This though needs further
400 investigation.

401 As equation 11 appears to successfully predict the reduction in vertical base resistance due to rotation
402 for the conical tip of different apex angles, it was then compared to the results of the 60° cone installed
403 using DEM at different installation pitches (Figure 11d). The analytical equation fits the results well,
404 for the conical tip. It should also be noted that as previously discussed the analytical model is unable
405 to predict the reductions of the flat base due to a potential difference in mechanism. Thus, showing
406 that by changing the base of the pile from a flat base to a 60° conical tip and rotary installing at $P_i > 8$,
407 a reduction in base resistance of 67% is possible (Figure 11c & d).

408 The proposed analytical model predicts the increase in the base component of the installation torque
409 (Equation 12). Similar to Equation 11, Equation 12 compares the base torque to $q_{b,0}$. To normalise the
410 base component of torque in terms of q_c , S is required. Figure 11e shows the normalised base torque
411 against β . The results show that with an increase in apex angle, there is an increase in normalised
412 torque, which agrees with the analytical solution in Equation 12. Although the normalised torque is
413 low for small apex angles, the value of base torque is larger than the torque for the shallow apex
414 angles. This is due to the increased surface area associated with small apex angles. It can also be seen
415 in Figure 11e, that the normalised base torque for the flat base matches the centrifuge test of Deeks
416 (2008). Figure 11f shows that Equation 12 is able to capture the behaviour of the normalised torque
417 for the 60° cone installed at different installation pitches.

418 The analytical solutions (Equation 11 & 12) compare well with the DEM, with only the flat base, from
419 both DEM and the centrifuge tests, showing some small variations against the analytical model. The

420 results show that it is possible to reduce the base resistance significantly by changing from a flat base
 421 to a conical tip. The conical tip will increase the base component of installation torque, but the base
 422 component remains relatively low in comparison with the shaft contribution to installation torque.

423 **5 Modification of the CPT prediction method to incorporate installation** 424 **pitch and base geometry**

425 Using the relationships obtained through this investigation it is now possible to modify the base and
 426 shaft components of the *CPT* based prediction method for installation torque and installation force
 427 originally proposed by Davidson *et al.* (2018) and Al-Baghdadi (2017), respectively. The updated
 428 equations include additional terms to add the effects of installation pitch and base geometry. The
 429 installation torque can be predicted using the following equations:

$$T = T_b + T_s \quad (14)$$

$$T_b = \bar{q}_c S \pi \frac{d_c^3 \tan \beta \tan \delta}{12 \sin \beta \tan \beta + \tan \delta} \left(\left[1 - 2 \left(\frac{\cos \beta}{P_i} \right)^2 \right] \sqrt{1 + \left(\frac{\cos \beta}{P_i} \right)^2} + 2 \left(\frac{\cos \beta}{P_i} \right)^3 \right) \quad (15)$$

$$T_s = \sum_{\Delta x=1}^{\Delta x_i=L} a \bar{q}_c \tan \delta \pi \Delta x d_c \frac{P_i}{\sqrt{1 + P_i^2}} f \quad (16)$$

$$f = 0.63 D_r + 0.52 \quad (17)$$

$$a = \frac{F_r}{\tan \delta} \quad (18)$$

$$P_i = \frac{\theta d_c}{2 \dot{w}} \quad (19)$$

$$S = 0.013 \beta + 0.6 \quad (20)$$

430 where T is the total torque resulting during installation, T_b is the torque associated with the base of
 431 the pile, T_s is the torque associated with the shaft of the pile, \bar{q}_c is the average value of q_c over a depth

432 of $3d_c$ ($1.5d_c$ above and below), β is half of the apex angle of the pile tip (for a flat base $\beta=90^\circ$) and S is
 433 the shape function for the base of the pile.

434 To predict the installation force the following equations are used:

$$F = F_b + F_s \quad (21)$$

$$F_b = \bar{q}_c S \pi \frac{d_c^2}{4} \left(\frac{\tan\beta}{\tan\beta + \tan\delta} + \frac{2 \tan\delta \cos\beta}{(\tan\beta + \tan\delta) \sqrt{\cos^2\beta + P_i^2 + \cos\beta}} \right) \quad (22)$$

$$F_s = \sum_{\Delta x=1}^{\Delta xi=L} \bar{a} \bar{q}_c \tan(\delta) \pi \Delta x d_c \frac{1}{\sqrt{1 + P_i^2}} \quad (23)$$

435 where F is the total force encountered during installation, F_b is the force attributed to the base of the
 436 pile, F_s is the force generated through shear resistance on the shaft of the pile. When calculating the
 437 base resistance for a rotary installed pile with a flat base, a 10% reduction in q_b should be considered
 438 in place of Equation 22 for piles installed at $P_i > 4$. This is due to the analytical solution used to
 439 formulate Equation 22 being unable to capture the behaviour of the flat base. The installation
 440 requirements for the shaft are calculated from the sum of intervals of length Δx (Figure 1a) over the
 441 total length of the pile. Although f should be present in Equation 23, the parameter has been omitted
 442 for simplicity. This is due to the negligible contribution of the shaft to the installation force at $P_i > 1$
 443 (Table 4).

444 5.1 Model-scale pile torque and force predictions

445 The proposed methods were used to predict the installation torque and force of a model pile installed
 446 in medium dense HST95 sand. The installation pitch of the 50g centrifuge test was 3.97 and the total
 447 torque and force were recorded with depth. The pile was 200 mm in length with an apex angle of 60° .
 448 CPT cone resistance data in the same density of sand was recorded in the centrifuge tests and can be
 449 seen in Figure 13a. Figure 13b&c shows the comparison between the predicted and measured values
 450 for both Installation force and torque. The predictions using the proposed equations show a good
 451 correlation with the measured values for both the torque and force, predictions using the original

452 equations reported in Al-Baghdadi (2017) and Davidson *et al.* (2018) can also be seen to over predict
453 installation requirements (Figure 13b&c). Showing that the proposed changes to the CPT installation
454 prediction method are better at predicting installation requirements.

455 **6 Conclusions**

456 The introduction of restrictions upon the allowable level of noise generated when installing deep
457 foundations offshore has increased the demand for “silent” piling techniques to be developed for the
458 offshore environment. One potential onshore silent piling technique that may be exported offshore is
459 the rotary installation of steel displacement piles, such as the rotary press-in method for tubular piles
460 or the installation of screw piles. Methods for predicting the installation requirements of rotary
461 installed straight shafted piles are limited, although several have previously been developed for small
462 scale onshore screw piles which may not be adequate for larger geometries. The effect of installation
463 pitch and base geometry, on the base and shaft components of installation force and torque has been
464 investigated for straight shafted piles in multiple relative densities using the DEM technique. The DEM
465 simulations conducted within this paper have been calibrated and validated against physical triaxial
466 and centrifuge tests.

467 From the investigation it can be concluded that it is possible to significantly reduce the vertical
468 installation force (or crowd) of a straight shafted pile by increasing the installation pitch in all relative
469 densities. Simulations conducted on a straight shafted pile with an apex angle of 60° , showed a
470 reduction in vertical base and shaft resistance of 34% and 85% respectively at $P_i > 8$. The installation
471 torque that is generated when the pile is rotated, is primarily produced by the shaft of the pile. The
472 installation torque increases with installation pitch although the increase in installation torque is
473 negligible at $P_i > 4$. Therefore, it is much more beneficial for rotary installed piles to be installed at P_i
474 > 8 . A reduction in shaft resistance during installation was discovered, with the percentage reduction
475 being larger in loose soil and much smaller in denser soils.

476 Comparisons against independent centrifuge tests highlighted that the geometry of the pile base
477 affected the base components of installation torque and force. Flat based piles were found to increase
478 the resistance to penetration by nearly double when installed through the press in method (no
479 rotation). Moreover, the percentage reduction in installation force and increase in installation torque
480 during rotary installation are significantly influenced by the base geometry. This led to the
481 development of an analytical solution for predicting the change in the base component of the
482 installation requirements for conical base geometries. It was found that 40° is the optimum apex angle
483 for the base of the pile, reducing the installation force significantly while maintaining a relatively low
484 torque.

485 Using the results of the DEM simulations and the analytical model, modifications to the base and shaft
486 components of the existing *CPT* based predictions methods for installation torque and force proposed
487 by Davidson *et al.* (2018) and Al-Baghdadi (2017) respectively have been improved to include the
488 effects of varying installation pitch and pile base geometry. The improved method will aid in the
489 prediction of the installation requirements and plant development for large offshore “silent” pile
490 deployment.

491

492 **7 Acknowledgements**

493 This research is a part of an EPSRC NPIF funded studentship with Roger Bullivant Limited The 4th
494 author is supported by the European Union’s Horizon 2020 research and innovation programme under
495 the Marie Skłodowska-Curie grant agreement No 753156. The authors would also like to acknowledge
496 the support of EPSRC (Grant no. EP/N006054/1: Supergen Wind Hub: Grand Challenges Project: Screw
497 piles for wind energy foundations).

498

499 **Table captions**

500 Table 1: HST95 sand physical and numerical properties (Sharif et al, 2019a)

501 Table 2: Properties of the virtual soil chambers used in this study at different relative densities

502 Table 3: Overview of simulations conducted in this study.

503 Table 4: Percentage contribution to installation requirements from base and shaft for all soil densities

504 **Figure captions**

505 Figure 1: a) Schematic of the geometry of the pile used by (Al-Baghdadi, 2017) and in the DEM
506 simulations (model scale dimensions in brackets) b) Example soil chamber used in DEM simulations,
507 shading indicates the particle size distribution scaling applied, diameter 25 m (0.5m), height 20 m
508 (0.4m) and $D_r = 73\%$ (gravitational acceleration 50g.)

509 Figure 2: Mean effective stress with depth below ground level at different radial distances from an
510 installed pile ($P_i = 0$ $D_r = 73\%$).

511 Figure 3: Comparison of DEM results for medium dense sand at varying installation pitch, a) total
512 vertical force vs penetration depth, b) total torque vs penetration depth

513 Figure 4: Schematic diagram of a rotary installed pile, showing the component and direction of shear
514 stresses acting on a straight shafted pile during rotary installation.

515 Figure 5: Comparison of normalised vertical stress results versus increasing installation pitch a)
516 normalised base resistance (q_b/q_c) b) Normalised shaft resistance (τ_{sv}/q_c) c) Comparison of the radial
517 stress distribution along the shaft of an installed pile and CPT in the dense soil bed ($D_r = 73\%$) d)
518 Comparison of equation 7 to the normalised shaft resistance from DEM and independent centrifuge
519 tests of Deeks (2008).

520 Figure 6: Normalised installation torque vs installation pitch a) base component of torque b) shaft
521 component of torque.

522 Figure 7: Comparison of normalised radial stress on the pile shaft for various installation pitches a)
523 loose b) medium dense c) dense d) Rotation reduction factor for radial stress on the pile shaft vs
524 relative density.

525 Figure 8: Comparison of particle displacement during installation at $P_i = 0$ & 4 for 0.25m of pile vertical
526 movement. (Particles are shaded by displacement in polar axis) a) Loose soil bed radial displacement
527 b) Loose soil bed rotational displacement c) Dense soil bed radial displacement d) Dense soil bed
528 rotational displacement

529 Figure 9: Comparison of normalised shaft resistance from DEM and independent centrifuge test of
530 Deeks (2008), with the inclusion of the rotation reduction factor, to Equation 10.

531 Figure 10: Comparison of base component of installation requirements between DEM and
532 independent centrifuge tests of Deeks (2008) a) Installation force b) Installation torque

533 Figure 11: Comparison of equation 11 and 12 to DEM and independent centrifuge tests of Deeks
534 (2008) a) Diagram of possible tip geometries b) normalised base resistance for pushed in pile with
535 different base geometries c) normalised base resistance against pile tip angle, β d) normalised base
536 resistance against installation pitch e) normalised base torque against pile tip angle, β f) normalised
537 base torque against installation pitch.

538 Figure 12 Average particle displacement below the base of an advancing flat based pile. a) Installation
539 pitch = 0, b) Installation pitch = 4.

540 Figure 13: Prediction of installation requirements of a rotary installed straight shafted pile. Installed
541 at $P_i = 3.97$ in centrifuge test from CPT Cone tip resistance, a) CPT Cone tip resistance from CPT
542 conducted in the geotechnical centrifuge ($D_r = 55\%$), b) Predicted vs measured prototype installation
543 force, c) Predicted vs measured prototype Installation torque.

544

545 **References**

- 546 Al-Baghdadi, T. (2017) *Screw piles as offshore foundations : Numerical and physical modelling*. Ph.D,
547 University of Dundee.
- 548 Al-Defae, A. H., Caucis, K. and Knappett, J. A. (2013) Aftershocks and the whole-life seismic
549 performance of granular slopes, *Géotechnique*. Thomas Telford Ltd, 63(14), pp. 1230–1244. doi:
550 10.1680/geot.12.P.149.
- 551 Arroyo, M., Butlanska, J., Gens, A., Calvetti, F. and Jamiolkowski, M. (2011) Cone penetration tests in
552 a virtual chamber, *Géotechnique*, 61(6), pp. 525–531. doi: 10.1680/geot.9.P.067.
- 553 Bolton, M. D., Gui, M. W., Garnier, J., Corte, J. F., Bagge, G., Laue, J. L. and Renzil, R. (1999)
554 Centrifuge cone penetration tests in sand, *Géotechnique*, 49(4), pp. 543–552. doi:
555 10.1680/geot.1999.49.4.543.
- 556 BS5228 (1992) *Noise control on construction and open sites - Part 4: Code of practice for noise and*
557 *vibration control applicable to piling operations*. London, United Kingdom, British Standards
558 Institute.
- 559 Butlanska, J., Arroyo, M., Gens, A. and O’Sullivan, C. (2014) Multiscale analysis of CPT in a virtual
560 calibration chamber, *Canadian Geotechnical Journal*, 26(1), pp. 80–86. doi: 10.1139/cgj-2012-0476.
- 561 Ciantia, M. O., Boschi, K., Shire, T. and Emam, S. (2018) Numerical techniques for fast generation of
562 large discrete-element models, *Proceedings of the Institution of Civil Engineers - Engineering and*
563 *Computational Mechanics*, 171(4), pp. 147–161. doi: 10.1680/jencm.18.00025.
- 564 Ciantia, M. O., O’Sullivan, C. and Jardine, R. (2019) Pile penetration in crushable soils: Insights from
565 micromechanical modelling, in *XVII ECSMGE-2019*. Reykjavik, Iceland, pp. 298–317. doi: doi:
566 10.32075/17ECSMGE-2019-1111.
- 567 Coyne, J. C. and Lewis, G. W. (1999) Analysis of plowing forces for a finite-width blade in dense,
568 ocean bottom sand, in *Oceans ’99 Riding the Crest into the 21st Century*. Seattle WA, USA: IEEE, pp.

569 1–10.

570 Davidson, C., Al-Baghdadi, T., Brown, M. J., Brennan, A., Knappett, J., Augarde, C. E., Coombs, W.,
571 Wang, L., Richards, D., Blake, A. and Ball, J. (2018) A modified CPT based installation torque
572 prediction for large screw piles in sand, in Hicks, M. A., Federico, P., and Peuchen, J. (eds) *Cone*
573 *Penetration Testing*. Delft, Netherlands: CRC Press, pp. 255–261. doi:
574 <https://doi.org/10.1201/9780429505980>.

575 Davidson, C., Brown, M. J., Cerfontaine, B., Knappett, J. A., Brennan, A. J., Al-Baghdadi, T., Augarde,
576 C., Coombs, W., Wang, L., Blake, A., Richards, D. and Ball, Jonathan, D. (2020) *Feasibility of screw*
577 *piles for offshore jacket structures, Geotechnique Accepted subject to revision (03/07/20)*.

578 Deeks, A. D. (2008) *An investigation into the strength and stiffness of jacked piles in sand*. Ph.D,
579 University of Cambridge.

580 Deeks, A. D. and White, D. (2008) Centrifuge modelling of rotary jacked tubular piles ‘Gryopiling’, in
581 Brown, M., Bransby, M. F., Brennan, A., and Knappett, J. A. (eds) *Proceedings of the second BGA*
582 *International Conference on Foundations ICOF2008*. Dundee, United Kingdom: Bre Press, pp. 531–
583 544.

584 Garnier J, Gaudin, C., Springman, S. M., Culligan P, Goodings, D., Konig, D., Kutter, B., Phillips, R.,
585 Randolph, M. and Thorel, L. (2007) Catalogue of scaling laws and similitude questions in geotechnical
586 centrifuge modelling, *International Journal of Physical Modelling in Geotechnics*, 7(3), pp. 1–23.

587 Gavin, K., Doherty, P. and Spagnoli, G. (2013) Prediction of the installation torque resistance of large
588 diameter helical piles in dense sand., in Lutenegeger, A. J. (ed.) *1st Int. Geotechnical Symp. of Helical*
589 *Foundations*. Amherst, USA, pp. 131–140.

590 Ghaly, A. and Hanna, A. (1991) Experimental and theoretical studies on installation torque of screw
591 anchors, *Canadian Geotechnical Journal*, 28(3), pp. 353–364. doi: 10.1139/t91-046.

592 Golightly, C. (2014) Technical Paper : Tilting of monopiles Long, heavy and stiff, pushed beyond their

- 593 limits, *Ground Engineering*, January, pp. 20–23.
- 594 Huisman, M. (2019) Silent Foundation Concept: Helical Piles For Skirt and Pre-piled Jacket
595 Foundations, in Davidson, C. ;, Brown, M. J., Knappett, J. A., Brennan, A. J., Augarde, C. E., Coombs,
596 W. M., Wang, L., Richards, D., White, D. J., and Blake, A. (eds) *International Symposium on Screw*
597 *Piles for Energy Applications*. Dundee, United Kingdom, pp. 117–118. doi: 10.20933/100001123.
- 598 Ishihara, Y., Haigh, S. and Bolton, M. (2015) Estimating base resistance and N value in rotary press-in,
599 *Soils and Foundations*. Elsevier, 55(4), pp. 788–797. doi: 10.1016/j.sandf.2015.06.011.
- 600 Itasca Consulting Group, I. (2016) PFC 5.0. Minneapolis: Itasca Consulting Group, Inc.
- 601 Jardine, R. J., Lehane, B. M. and Everton, S. J. (1993) Friction Coefficients for Piles in Sands and Silts,
602 *Offshore Site Investigation and Foundation Behaviour*, 28(1), pp. 661–677. doi: 10.1007/978-94-017-
603 2473-9_31.
- 604 Jeffrey, J. R., Brown, M. J., Knappett, J. A., Ball, J. D. and Caucis, K. (2016) CHD pile performance: part
605 I – physical modelling, *Proceedings of the Institution of Civil Engineers - Geotechnical Engineering*,
606 169(5), pp. 421–435. doi: 10.1680/jgeen.15.00131.
- 607 Lauder, K. D., Brown, M. J., Bransby, M. F. and Boyes, S. (2013) The influence of incorporating a
608 forecutter on the performance of offshore pipeline ploughs, *Applied Ocean Research*, 39, pp. 121–
609 130. doi: 10.1016/j.apor.2012.11.001.
- 610 Lehane, B. M., Schneider, J. . and Xu, X. (2005) The UWA-05 method for prediction of axial capacity
611 of driven piles in sand, in *Proc. Int.Symp. Front. Offshre Geotech*. Perth, Australia, pp. 683–689.
- 612 Liu, J., Duan, N., Cui, L. and Zhu, N. (2019) DEM investigation of installation responses of jacked
613 open-ended piles, *Acta Geotechnica*. Springer Berlin Heidelberg, pp. 1–15. doi: 10.1007/s11440-019-
614 00817-7.
- 615 Lutenegger, A. J. (2009) Cylindrical shear or plate bearing - Uplift behavior of multi-helix screw

- 616 anchors in clay, in *Geotechnical Special Publication*, pp. 456–463. doi: 10.1061/41021(335)57.
- 617 Lutenegger, A. J. (2019) Screw Piles and Helical Anchors- What we Know and What we Don't Know:
618 An Academic Perspective - 2019, in Davidson, C. ;, Brown, M. J., Knappett, J. A., Brennan, A. J.,
619 Augarde, C. E., Coombs, W. M., Wang, L., Richards, D., White, D. J., and Blake, A. (eds) *ISSPEA*.
620 Dundee, UK: University of Dundee, pp. 15–28. doi: 10.20933\100001123.
- 621 Mandolini, A., Ramondini, M., Russo, G. and Viggiani, C. (2002) Full scale loading tests on
622 instrumented CFA piles, in *Geotechnical Special Publication*, pp. 1088–1097. doi:
623 10.1061/40601(256)77.
- 624 McDowell, G. R., Falagush, O. and Yu, H.-S. (2012) A particle refinement method for simulating DEM
625 of cone penetration testing in granular materials, *Géotechnique Letters*. Thomas Telford Ltd, 2(3),
626 pp. 141–147. doi: 10.1680/geolett.12.00036.
- 627 Mindlin, R. D. and Deresiewicz, H. (1953) Elastic spheres in contact under varying oblique forces,
628 *Journal of Applied Mechanics ASME*, 20, pp. 327–344. doi: 10.1007/978-1-4613-8865-4_35.
- 629 Robertson, P. K., Campanella, R. G., Gillespie, D. and Greig, J. (1986) Use of piezometer cone data, in
630 *ASCE Speciality Conference In Situ 1986*. Blacksburg, pp. 1263–1280.
- 631 Sakr, M. (2015) Relationship between Installation Torque and Axial Capacities of Helical Piles in
632 Cohesionless Soils, *Journal of Performance of Constructed Facilities*, 29(6), p. 04014173. doi:
633 10.1061/(ASCE)CF.1943-5509.0000621.
- 634 Schneider, J., Engineer, C. and White, D. J. (2007) Back analysis of Tokyo port bay bridge pipe pile
635 load tests using piezocone data, in *International Workshop on Recent Advances in Deep Foundations*.
636 Yokosuka, Japan, pp. 183–194. doi: 10.1201/9780203938416.ch11.
- 637 Sharif, Y., Brown, M. J., Ciantia, M., Knappett, J., Davidson, C., Cerfontaine, B., Robinson, S. and Ball,
638 J. (2019a) Numerically Modelling the Installation and loading of Screw Piles using DEM, in Davidson,
639 C. ;, Brown, M. J., Knappett, J. A., Brennan, A. J., Augarde, C. E., Coombs, W. M., Wang, L., Richards,

- 640 D., White, D. J., and Blake, A. (eds) *ISSPEA*. Dundee, UK: University of Dundee, pp. 101–108. doi:
641 10.20933/100001123.
- 642 Sharif, Y., Ciantia, M., Brown, M. J., Knappett, J. A. and Ball, J. D. (2019b) Numerical Techniques For
643 the Fast Generation of Samples Using the Particle Refinement Method, in *Proceedings of the 8th*
644 *International Conference on Discrete Element Methods*. Enschede, Netherlands, p. 181.
- 645 Shi, D., Yang, Y., Deng, Y. and Xue, J. (2019) DEM modelling of screw pile penetration in loose
646 granular assemblies considering the effect of drilling velocity ratio, *Granular Matter*. Springer Berlin
647 Heidelberg, 21(3), pp. 1–16. doi: 10.1007/s10035-019-0933-3.
- 648 Spagnoli, G. (2017) A CPT-based model to predict the installation torque of helical piles in sand,
649 *Marine Georesources and Geotechnology*. Taylor & Francis, 35(4), pp. 578–585. doi:
650 10.1080/1064119X.2016.1213337.
- 651 Tatsuoka, F., Sonoda, S., Hara, K., Fukushima, S. and Pradhan, T. B. S. (1986) Failure and Deformation
652 of Sand in Torsional Shear, *Soils and Foundations*, 26(4), pp. 79–97. doi:
653 doi.org/10.3208/sandf1972.26.4_79.
- 654 White, D. J. and Deeks, A. D. (2007) Recent research into the behaviour of jacked foundation piles,
655 *International Workshop on Recent Advances of Deep Foundations (IWDPF07)*, 7096(January), pp. 3–
656 26. doi: 10.3101/1098-7096(2007)68.
- 657 White, D., Schneider, J. and Lehane, B. (2005) The influence of effective area ratio on shaft friction of
658 displacement piles in sand, in Cassidy, M. J. and Gourvenec, S. (eds) *Proceedings of the International*
659 *Symposium on Frontiers in Offshore Geotechnics*. Perth, Australia: CRC Press/Balkema, pp. 741–747.
- 660

Notation

a	Stress drop index
b	percentage base resistance other than from friction
A_b	Surface area of pile base
A_s	Surface area of pile shaft
CFA	Continuous flight auger pile
CHD	Continuous helical displacement pile
CPT	Cone penetration test
d_{00}	Minimum particle size
d_{50}	Median particle size
d_{100}	Maximum particle size
d_c	Diameter of pile core
DEM	Discrete element modelling
D_r	Relative density
f	Radial stress reduction factor
F	Total Installation force
FEA	Finite element analysis
F_b	Installation force from base
F_h	Installation force from helix
F_r	CPT friction ratio
F_s	Installation force from shaft
f_s	Sleeve friction
k_0	Coefficient of earth pressure at rest
L	Length of the pile
n_i	Particle scaling value
N	Model scaling factor
P_g	Geometric pitch
P_i	Installation pitch
PRM	Particle refinement method
PSD	Particle size distribution
q_b	Base resistance
$q_{b,0}$	Base resistance of pile installed at $P_i = 0$
q_c	CPT cone resistance
q_c	average q_c over $3d_c$
q_{ca}	average CPT cone resistance
R	Radius of the pile
\bar{R}	average radius of cone
S	Shape function for pile base
T	Total installation torque
T_b	Base component of installation torque
T_h	Torque from helix
T_{hl}	Torque from lower surface of helix

T_{h2}	Torque from outer perimeter of helix
T_{h3}	Torque from leading edge of helix
T_s	Shaft component of installation torque
U	Magnitude of average particle displacement
\dot{w}	Vertical velocity of pile
X	Horizontal distance from pile centre
y	Depth below ground level
z	Penetration depth
β	Half of the apex angle of pile base
γ'	Effective unit weight of soil
δ	Interface friction angle
δ_r	Particle radial displacement
δ_{CPT}	Critical state friction angle of the CPT
δ_{pile}	Critical state friction angle of the Pile
δ_θ	Particle rotational displacement
$\dot{\theta}$	Rotational velocity
σ'	Mean effective stress
σ_r	Radial stress on the shaft of the pile
σ_n	Normal stress on interface of pile base
τ_b	Base shear stress
τ_{bt}	Tangential component of base shear stress
τ_{bv}	Vertical component of base shear stress
τ_s	Shaft shear stress
τ_{st}	Tangential component of shaft shear stress
τ_{sv}	Vertical component of shaft shear stress

Table 1: HST95 sand physical and numerical properties (Sharif et al, 2019a)

HST95 silica sand property	Value
<i>Physical properties</i>	
Sand unit weight γ (kN/m ³)	16.75
Minimum dry density γ_{\max} (kN/m ³)	14.59
Maximum dry density γ_{\min} (kN/m ³)	17.58
Critical state friction angle, ϕ (degrees)	32
Interface friction angle, δ (degrees)	18
D ₃₀ (mm)	0.12
D ₆₀ (mm)	0.14
<i>DEM Parameters</i>	
Shear modulus, G (GPa)	3
Friction coefficient, μ (-)	0.264
Poisson's ratio, ν (-)	0.3
Interface friction coefficient [pile], μ_{pile} (-)	0.16

Draft

Table 1: Properties of soil chambers used in this study at different relative densities (model scale parameters)

Property	Loose	Medium Dense	Dense
Relative Density (%)	32	55	72
Voids ratio (e)	0.67	0.60	0.55
Height (mm)	400	400	400
Radius (mm)	250	250	250
Core PSD scaling (N_c)	20	20	20
Gravitational field	50	50	50
Number of Particles	200,000	225,000	250,000
Pile Diameter (mm)	10	10	10
Cone penetrometer Diameter(mm)	10	10	10

Draft

Table 1: Overview of simulations conducted in this study

Test Number	Pile type	Relative density, D_r (%)	Installation Pitch, P_1 (-)	tip geometry (degrees)	β (degrees)
1	CPT	32	0	60	NA
2	Straight shafted pile	32	0	60	30
3	Straight shafted pile	32	0.5	60	30
4	Straight shafted pile	32	1	60	30
5	Straight shafted pile	32	4	60	30
6	Straight shafted pile	32	8	60	30
7	Straight shafted pile	32	10	60	30
8	CPT	55	0	60	NA
9	Straight shafted pile	55	0	60	30
10	Straight shafted pile	55	0.5	60	30
11	Straight shafted pile	55	1	60	30
12	Straight shafted pile	55	4	60	30
13	Straight shafted pile	55	8	60	30
14	Straight shafted pile	55	10	60	30
15	CPT	73	0	60	NA
16	Straight shafted pile	73	0	60	30
17	Straight shafted pile	73	0.5	60	30
18	Straight shafted pile	73	1	60	30
19	Straight shafted pile	73	4	60	30
20	Straight shafted pile	73	8	60	30
21	Straight shafted pile	73	10	60	30
22	Straight shafted pile	73	0	20	10
23	Straight shafted pile	73	0	40	20
24	Straight shafted pile	73	0	80	40
25	Straight shafted pile	73	0	180 (flat)	90
26	Straight shafted pile	73	4	20	10
27	Straight shafted pile	73	4	40	20
28	Straight shafted pile	73	4	80	40
29	Straight shafted pile	73	4	180 (flat)	90

Table 1: Percentage contribution to installation requirements from base and shaft for all soil densities

Installation Pitch	Installation Force F		Installation Torque T	
	Base (%) F_b	Shaft F_s (%)	Base T_b (%)	Shaft T_s (%)
0	75	25	0	0
0.5	80	20	39	61
1	82	18	37	63
4	90	10	38	62
8	94	6	40	60
10	95	5	39	61

Draft

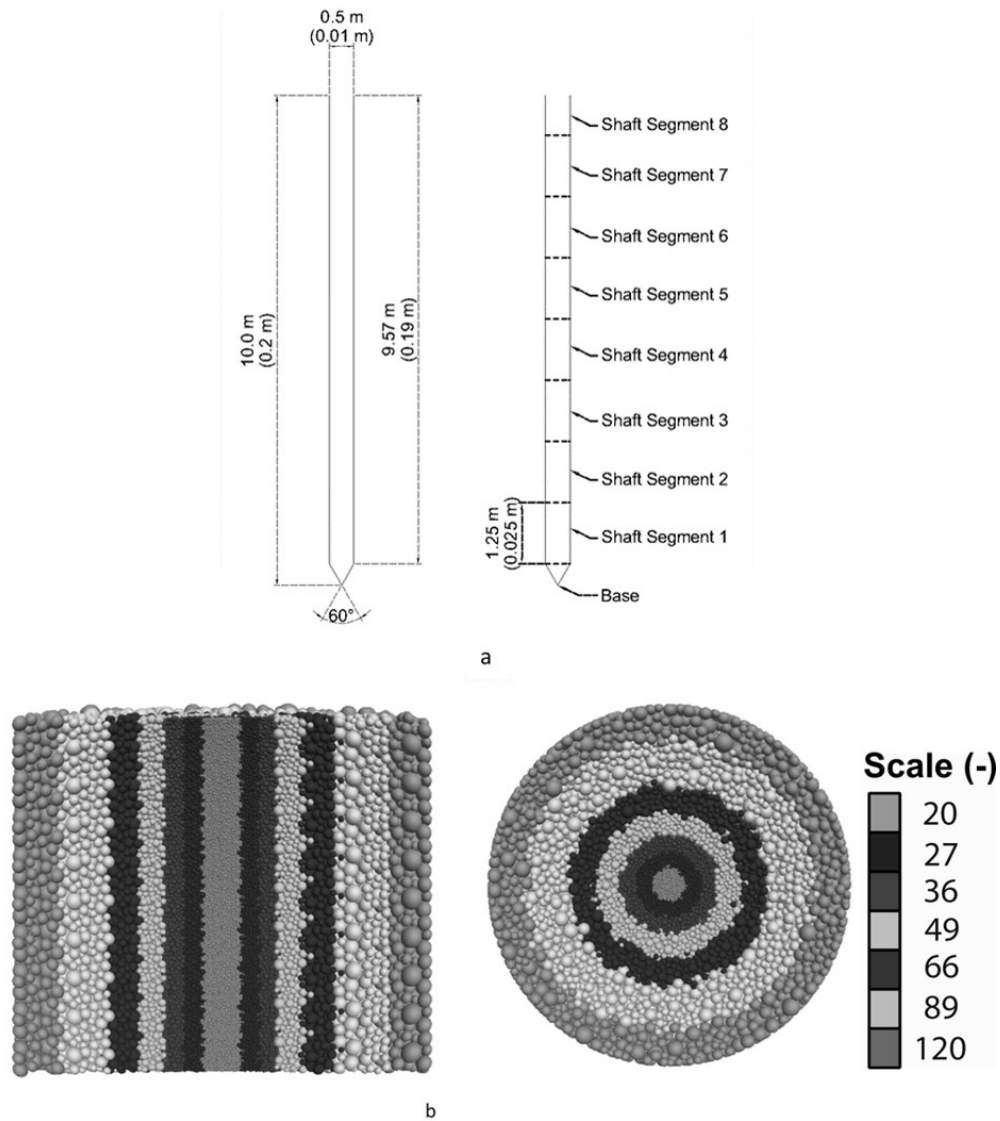


Figure 1: a) Schematic of the geometry of the pile used by (Al-Baghdadi, 2017) and in the DEM simulations (model scale dimensions in brackets) b) Example soil chamber used in DEM simulations, shading indicates the particle size distribution scaling applied, diameter 25 m (0.5 m), height 20 m (0.4 m) and $D_r = 73\%$ (gravitational acceleration 50g)

159x181mm (150 x 150 DPI)

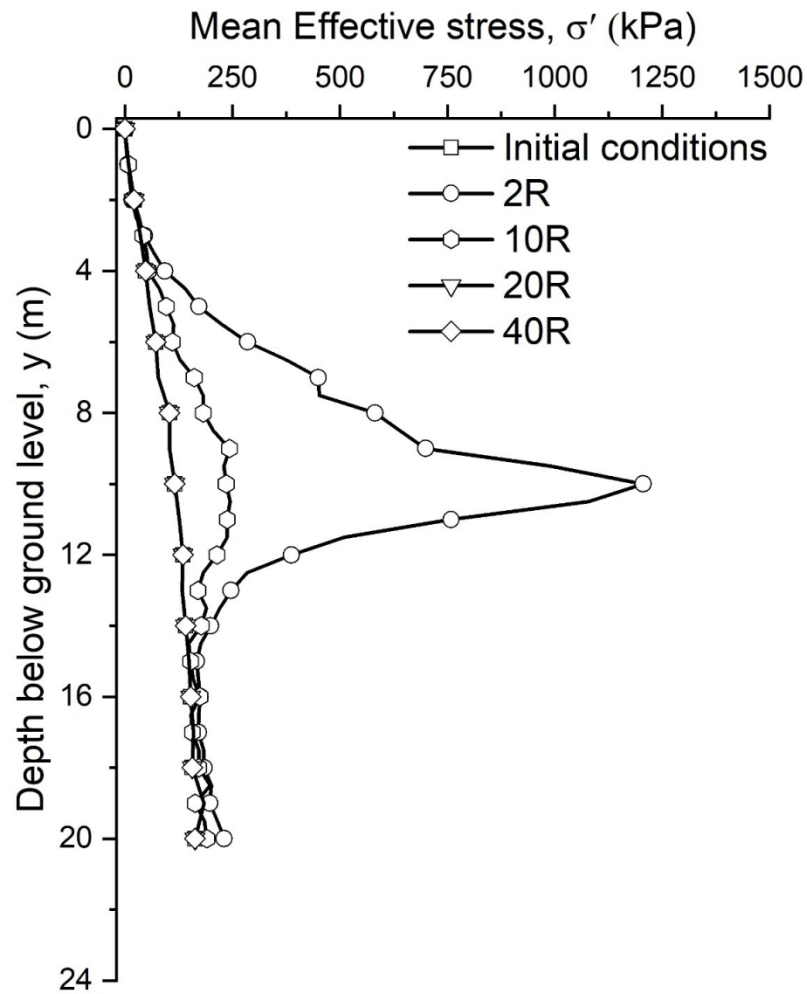


Figure 2: Mean effective stress with depth below ground level at different radial distances from an installed pile ($P_i = 0$ $D_r = 73\%$).

159x198mm (220 x 220 DPI)

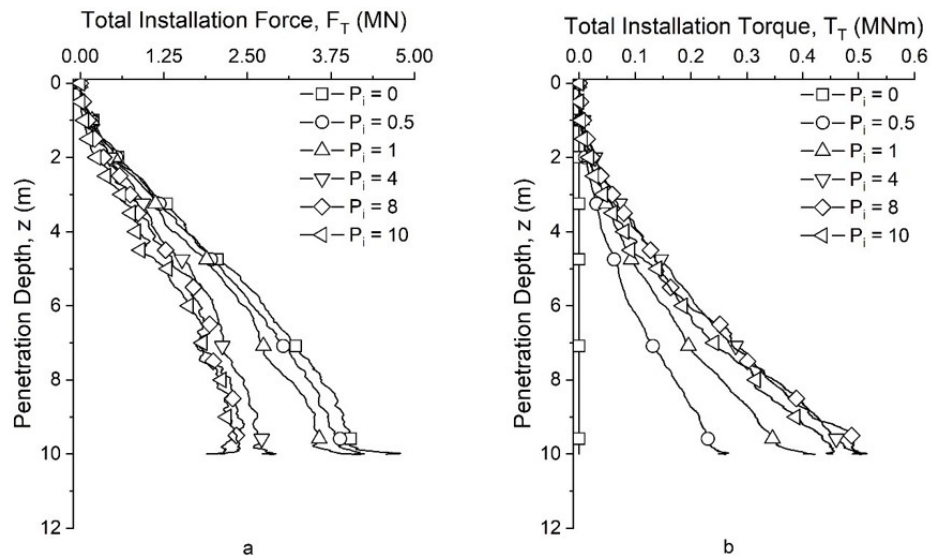


Figure 3: Comparison of DEM results for medium dense sand at varying installation pitch, a) total vertical force vs penetration depth, b) total torque vs penetration depth

158x98mm (150 x 150 DPI)

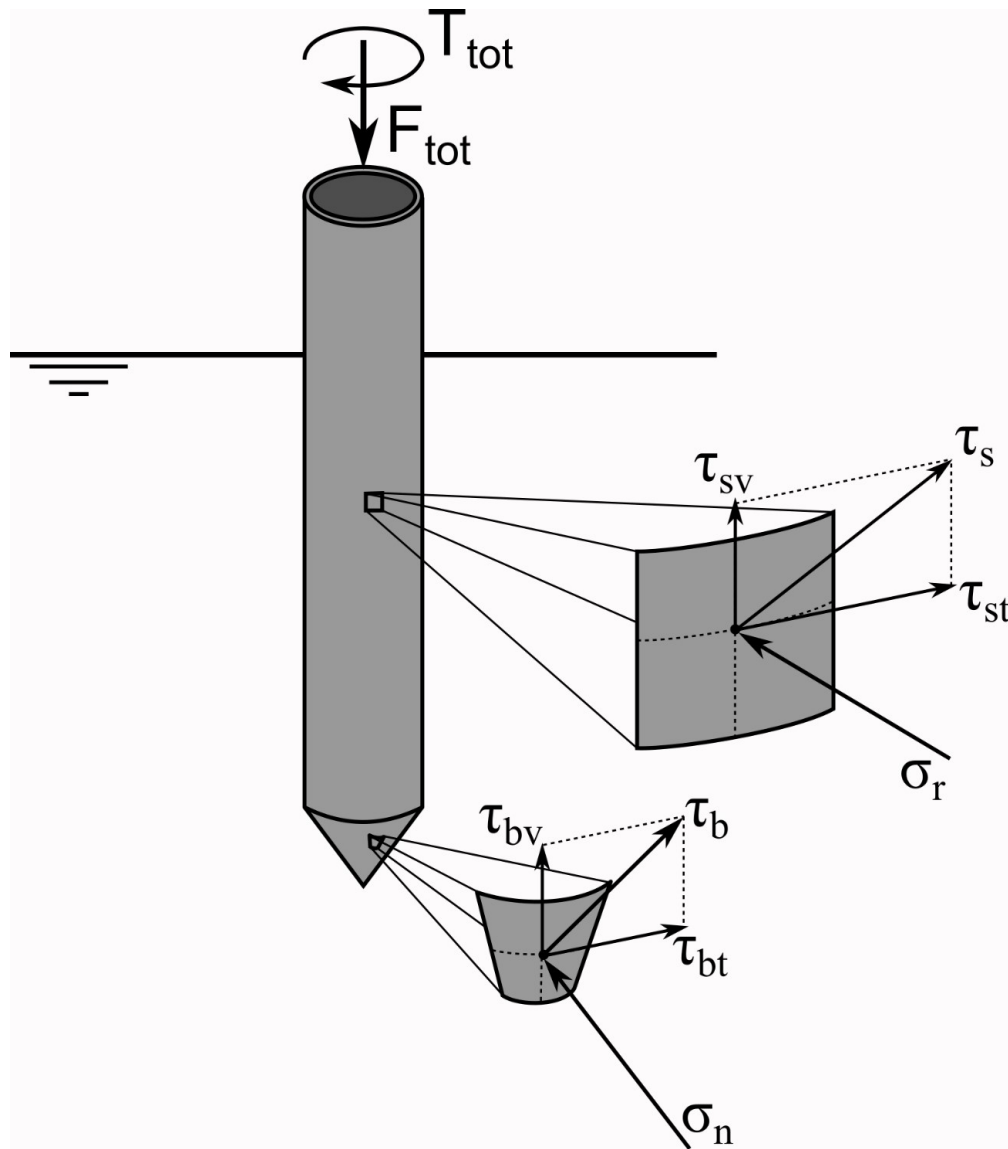


Figure 4: Schematic diagram of a rotary installed pile, showing the component and direction of shear stresses acting on a straight shafted pile during rotary installation.

149x170mm (220 x 220 DPI)

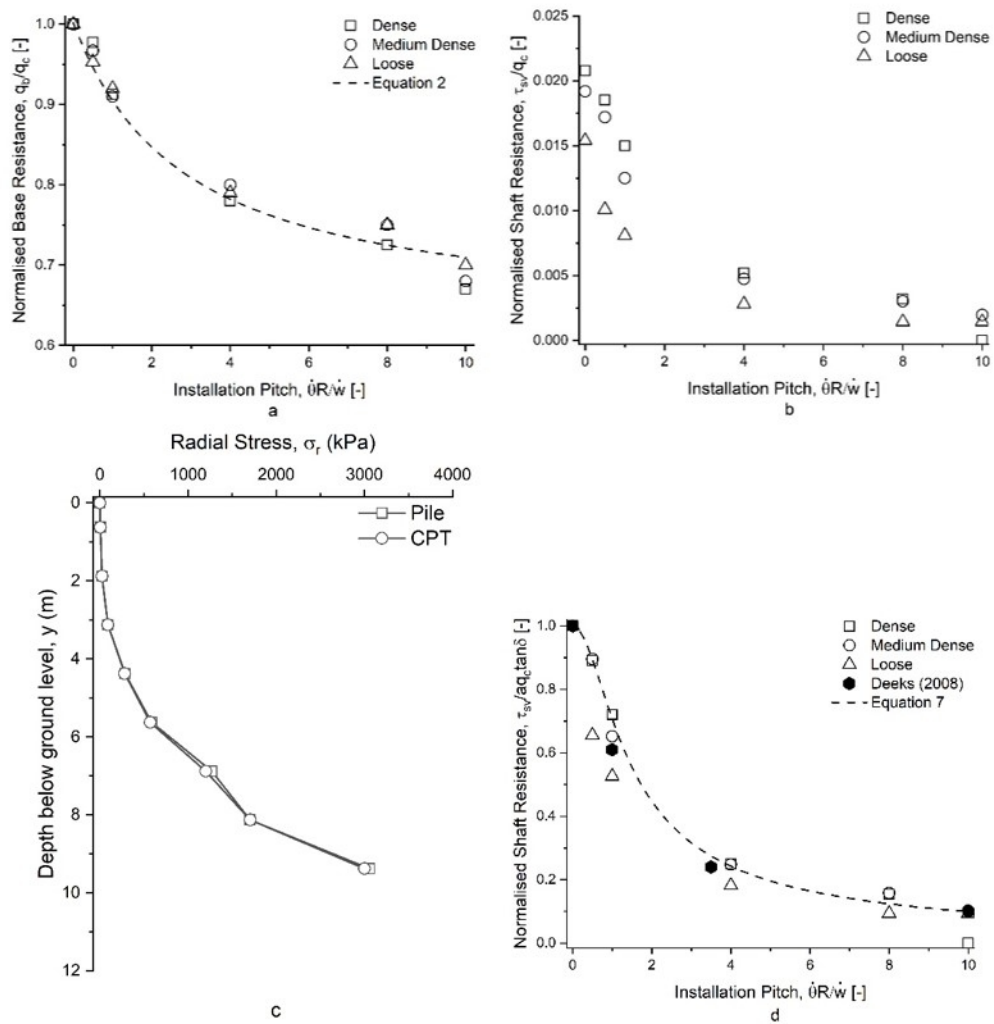


Figure 5: Comparison of normalised vertical stress results versus increasing installation pitch a) normalised base resistance (q_b/q_c) b) Normalised shaft resistance (τ_{sv}/q_c) c) Comparison of the radial stress distribution along the shaft of an installed pile and CPT in the dense soil bed ($D_r = 73\%$) d) Comparison of equation 7 to the normalised shaft resistance from DEM and independent centrifuge tests of Deeks (2008).

132x140mm (150 x 150 DPI)

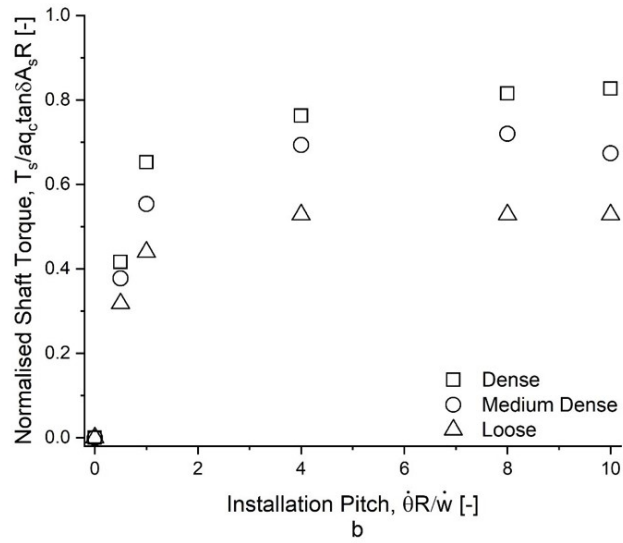
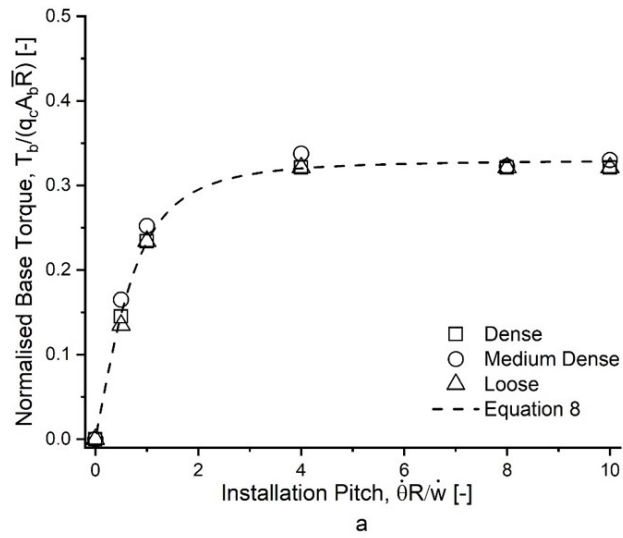


Figure 6: Normalised installation torque vs installation pitch a) base component of torque b) shaft component of torque

144x219mm (150 x 150 DPI)

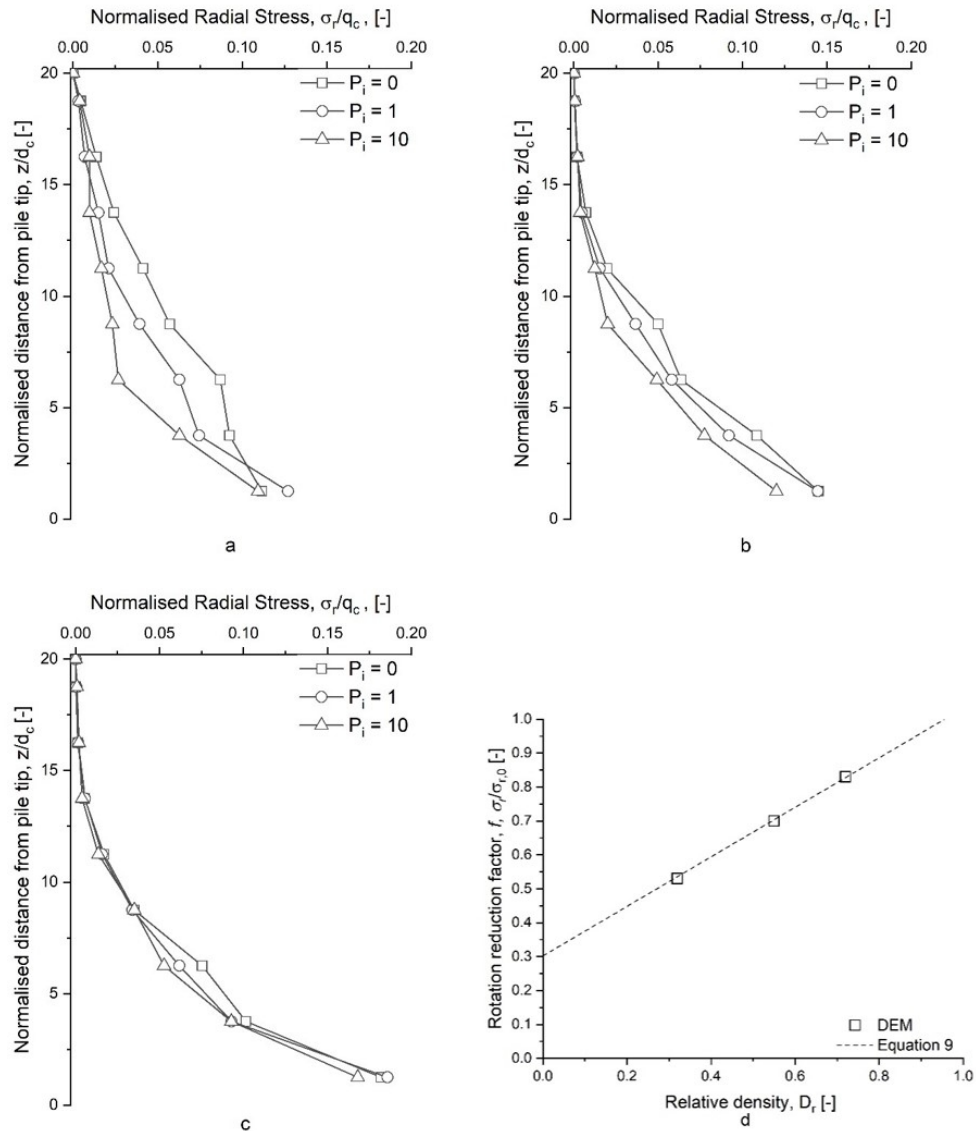


Figure 7: Comparison of normalised radial stress on the pile shaft for various installation pitches a) loose b) medium dense c) dense d) Rotation reduction factor for radial stress on the pile shaft vs relative density

155x177mm (150 x 150 DPI)

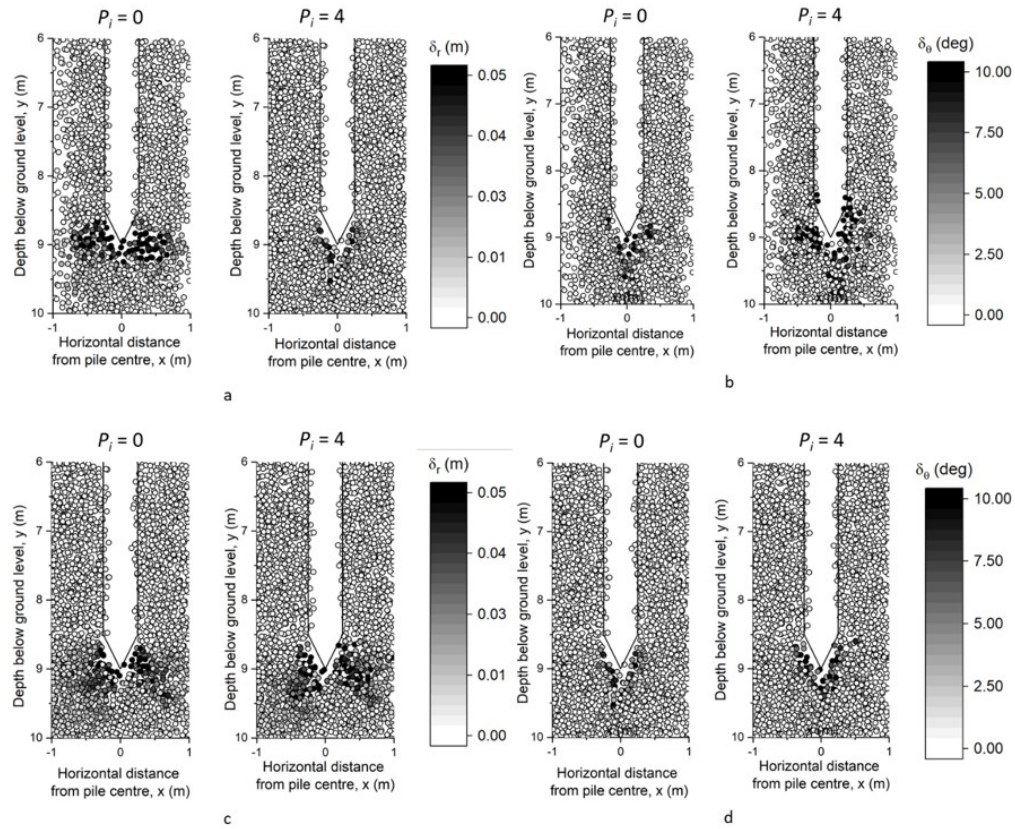


Figure 8: Comparison of particle displacement during installation at $P_i = 0$ & 4 for 0.25m of pile vertical movement. (Particles are shaded by displacement in polar axis) a) Loose soil bed radial displacement b) Loose soil bed rotational displacement c) Dense soil bed radial displacement d) Dense soil bed rotational displacement

149x126mm (150 x 150 DPI)

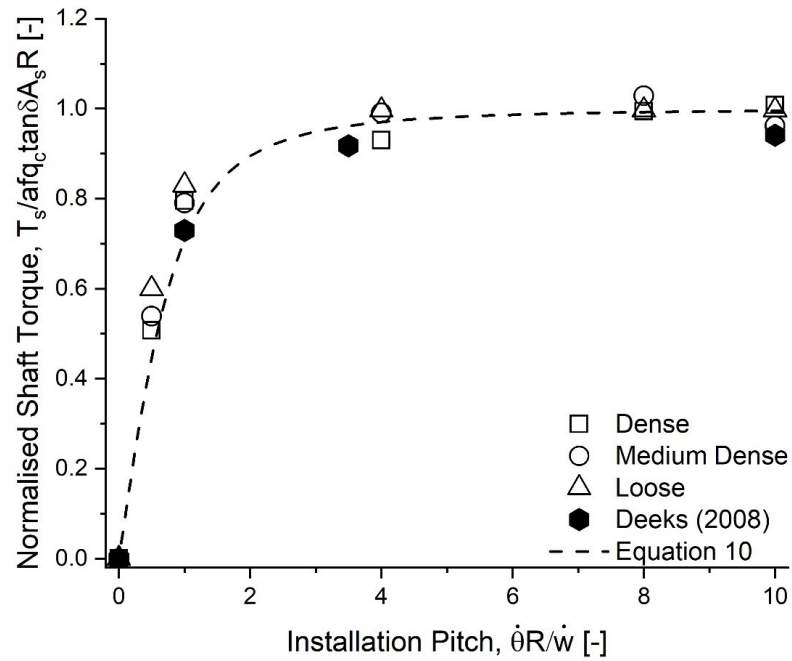


Figure 9: Comparison of normalised shaft resistance from DEM and independent centrifuge test of Deeks (2008), with the inclusion of the rotation reduction factor, to Equation 10

159x121mm (220 x 220 DPI)

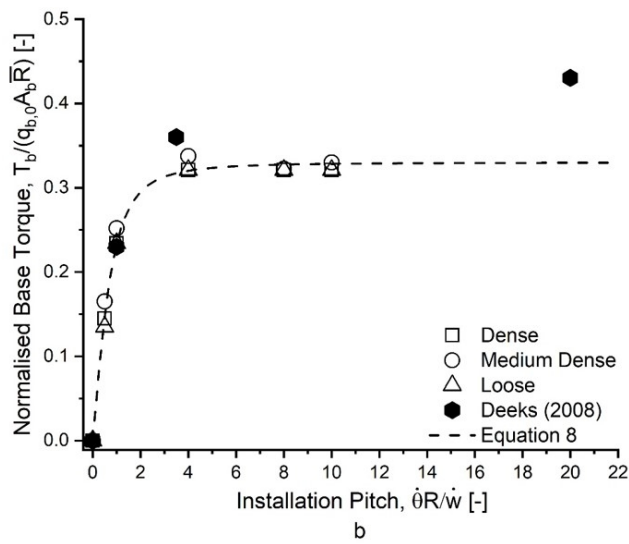
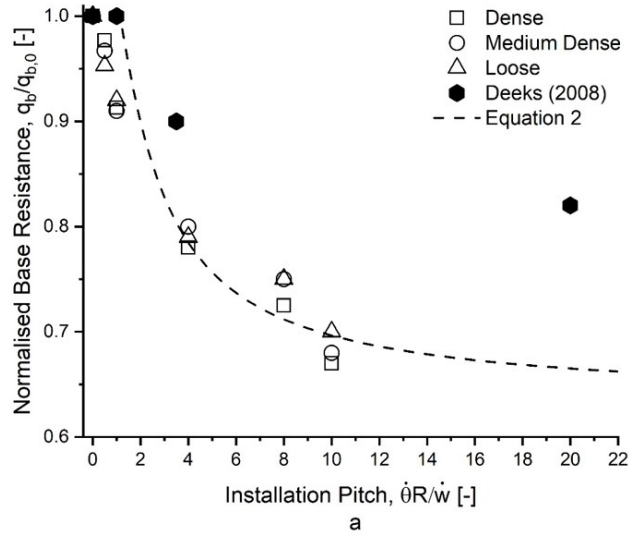


Figure 10: Comparison of base component of installation requirements between DEM and independent centrifuge tests of Deeks (2008) a) Installation force b) Installation torque

143x219mm (150 x 150 DPI)

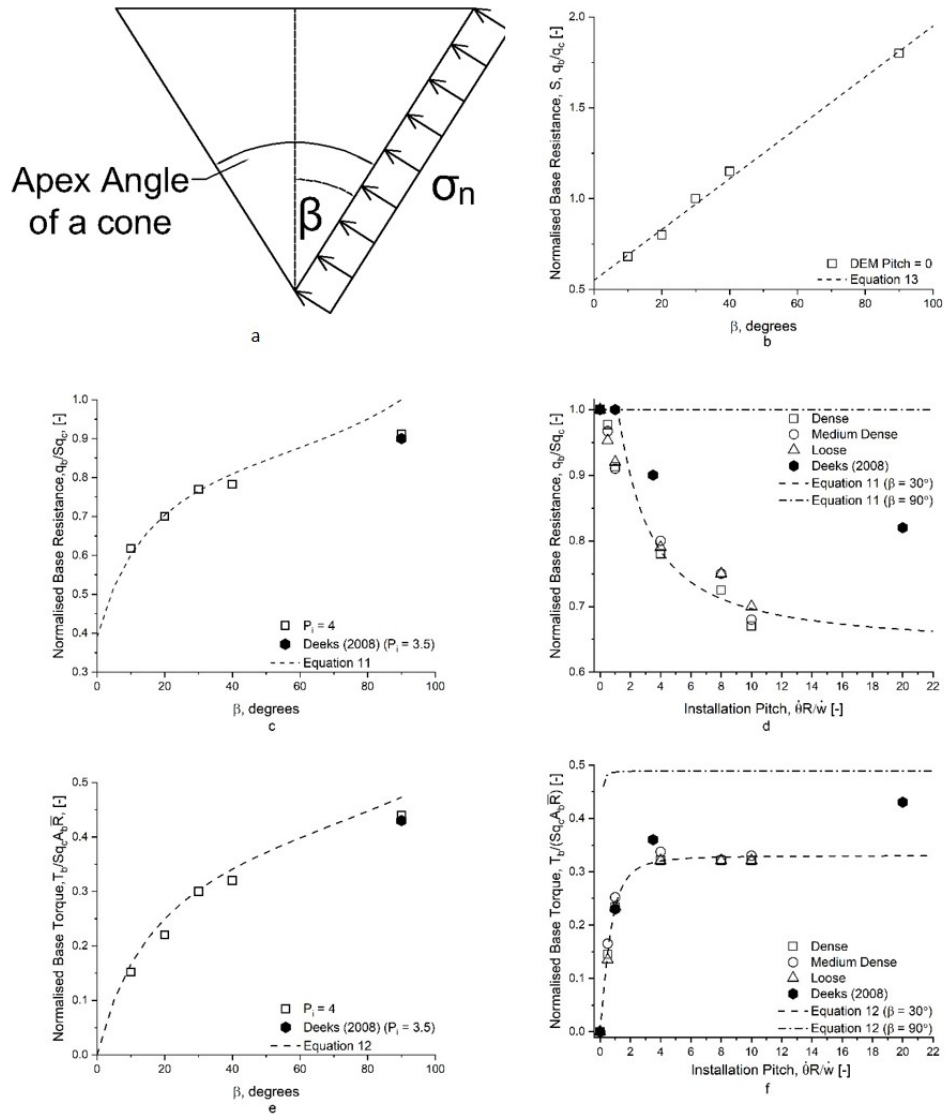


Figure 11: Comparison of Equation 11 and 12 to DEM and independent centrifuge tests of Deeks (2008) a) Diagram of possible tip geometries b) normalised base resistance for pushed in pile with different base geometries c) normalised base resistance against pile tip angle, β d) normalised base resistance against installation pitch e) normalised base torque against pile tip angle, β f) normalised base torque against installation pitch.

158x180mm (150 x 150 DPI)

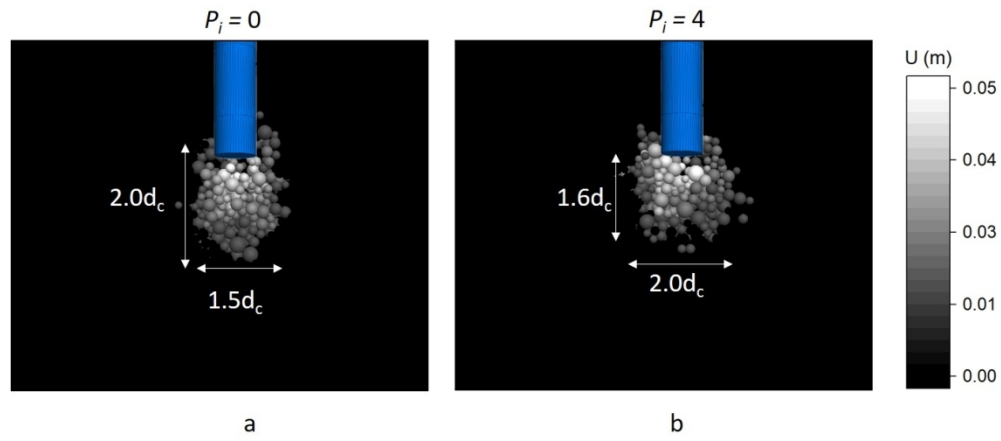


Figure 12 Average particle displacement below the base of an advancing flat based pile. a) Installation pitch = 0, b) Installation pitch = 4.

239x110mm (150 x 150 DPI)

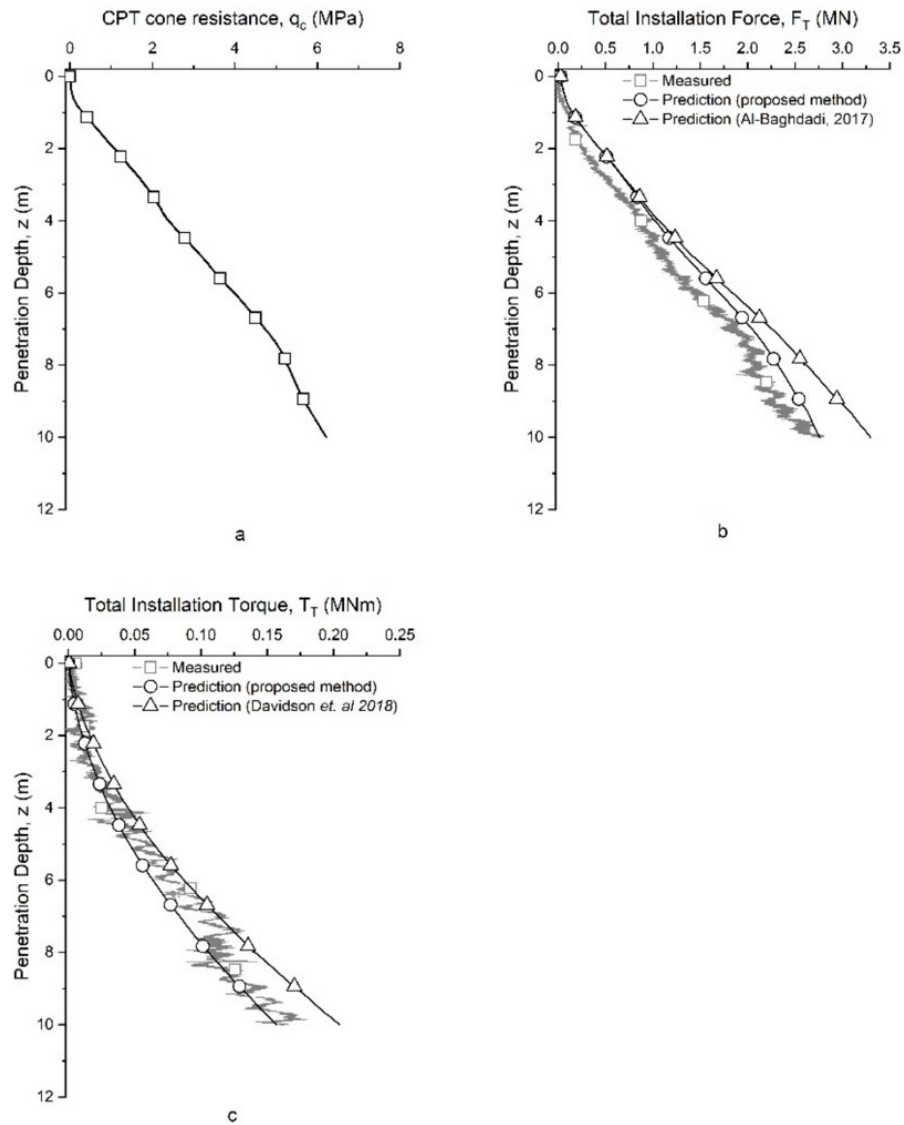


Figure 13: Prediction of installation requirements of a rotary installed straight shafted pile. Installed at $P_i = 3.97$ in centrifuge test from CPT Cone tip resistance, a) CPT Cone tip resistance from CPT conducted in the geotechnical centrifuge ($D_r = 55\%$), b) Predicted vs measured prototype installation force, c) Predicted vs measured prototype Installation torque.

150x183mm (150 x 150 DPI)